Landslide Susceptibility Zonation Using Statistical and Machine Learning Approaches in Northern Lecco, Italy

Mohammad Mehrabi (mohammad.mehrabi@mail.polimi.it)
Polytechnic of Milan - Lecco Campus: Politecnico di Milano - Polo territoriale di Lecco

Research Article

Keywords: Geo-hazard landslide, Susceptibility assessment, Frequency ratio, Artificial neural network, Neuro-fuzzy model

Posted Date: August 6th, 2021

DOI: https://doi.org/10.21203/rs.3.rs-771789/v1

Version of Record: A version of this preprint was published at Natural Hazards on November 10th, 2021. See the published version at https://doi.org/10.1007/s11069-021-05083-z.

Landslide Susceptibility Zonation Using Statistical and Machine Learning Approaches in Northern Lecco, Italy

Mohammad Mehrabi

Department of Civil and Environmental Engineering, Politecnico di Milano, Milan, Italy

Email: mohammad.mehrabi@mail.polimi.it

Abstract

This study deals with landslide susceptibility mapping in the northern part of Lecco Province, Lombardy Region, Italy. In so doing, a valid landslide inventory map and thirteen conditioning factors (including elevation, slope aspect, slope degree, plan curvature, profile curvature, distance to waterway, distance to road, distance to fault, soil type, land use, lithology, stream power index, and topographic wetness index) form the spatial database within geographic information system (GIS). The used evaluative models comprise a bivariate statistical approach called frequency ratio (FR) and two machine learning tools, namely multi-layer perceptron neural network (MLPNN) and adaptive neuro-fuzzy inference system (ANFIS). These models first use landslide and non-landslide records for comprehending the relationship between the landslide occurrence and conditioning factors. Then landslide susceptibility values are predicted for the whole area. The accuracy of the produced susceptibility maps is measured using area under the curve (AUC) index, according to which, the MLPNN (AUC = 0.916) presented the most accurate map, followed by the FR (AUC = 0. 898) and ANFIS (AUC = 0.889). Visual interpretation of the susceptibility maps, FR-based correlation analysis, as well as the importance assessment of conditioning factors, all indicated the significant contribution of the road networks to the crucial susceptibility of landslide. Lastly, an explicit predictive formula is extracted from the implemented MLPNN model for a convenient approximation of landslide susceptibility value.

Keywords: Geo-hazard landslide; Susceptibility assessment; Frequency ratio; Artificial neural network; Neuro-fuzzy model.

1 Introduction

Landslide is a ubiquitous environmental disaster that is responsible for nearly 17% of life losses and exclusively accounts for about 5% of the natural catastrophes worldwide (Kjekstad and Highland 2009, Pham et al. 2019). Different definitions and classification systems have been proposed for landslides (Li and Mo 2019). Cruden (1991), for instance, explained landslide as mass movements of rock, earth or debris down a slope. It may not be feasible to stop or control the landslide. Nevertheless, utilizing decision support systems for recognizing landslide-prone areas is an effective way toward mitigating the corresponding damages (Thai Pham et al. 2019).

Landslide is a dynamic phenomenon (Pandey et al. 2021) whose susceptibility assessment requires taking the effect of several parameters into consideration (Hua et al. 2021). Due to this reason, scholars have tested various strategies such as statistical analysis (Reichenbach et al. 2018), decision making (Yoshimatsu and Abe 2006), and soft computing (Huang and Zhao 2018) for susceptibility (and hazard) assessment of landslide (Catani et al. 2005). Yalcin (2008) used three models including analytical hierarchy process (AHP), statistical index (SI), and weighting factor for landslide susceptibility mapping at Ardesen region, Turkey. Regmi et al. (2014) examined the efficiency of the FR, SI, and weights-of-evidence for mapping the susceptibility of landslide in central regions of Nepal Himalaya. It was shown that the FR with success rate and predictive accuracy of 76.8% and of 75.4%, respectively, performed better than two other models. The applicability of decision-making models has been investigated in various studies (Mirdda et al. 2020, Maqsoom et al. 2021, Pham et al. 2021). Pourghasemi et al. (2012) produced the landslide susceptibility map of the Safarood Basin, located in the Northern part of Iran, using index of entropy and conditional probability techniques. Both models presented higher than 82% accuracy which indicates the reliability of the maps.

Machine learning models have greatly assisted engineers in coping with many non-linear problems, including the evaluation of environmental phenomena like forest fire (Bui et al. 2019), flood (Al-Abadi 2018), groundwater potential (Naghibi et al. 2016), gully erosion (Gayen et al. 2019), etc. Recent decades have witnessed the increasing popularity of various machine learning models. Logistic regression (LR) (Ayalew and Yamagishi 2005), boosting algorithms (Sahin 2020), support vector machine (Pourghasemi et al. 2013), tree-based approaches (Hong et al. 2018), and neighbor-based methods (El-Magd et al. 2021) are some of the well-known machine learning models that have been effectively used for landslide-related analysis, particularly susceptibility assessments.

Artificial neural network (ANN) and adaptive neuro-fuzzy inference system (ANFIS) are other notions of soft computing that have powerfully served for exploring non-linear engineering parameters. These models use sophisticated algorithms to dig and learn the pattern of the intended parameters. Pradhan et al. (2010) and Lee et al. (2003) tested and professed the feasibility of ANNs for landslide susceptibility mapping. Similar evaluations have been reported by Oh and Pradhan (2011) and Vahidnia et al. (2010) for the ANFIS. Jacinth Jennifer and Saravanan (2021) manifested a successful application of ANNs for susceptibility estimation of landslide in Idukki district of India. It was observed that the ANN models with a more complex structure achieved above 90% accuracy of prediction. Mehrabi et al. (2020) trained an ANFIS model using metaheuristic approaches. They showed that genetic algorithm (GA) is a suitable algorithm for optimizing the parameters of membership functions in ANFIS. In research by Hong et al. (2020), the GA showed nice performance also for supervising multi-layer perceptron neural network (MLPNN). Further applications of the MLPNN model for predicting environmental threats can be found in (Yi et al. 2020, Avand and Moradi 2021, Mohajane et al. 2021).

Comparative studies have always released valuable findings toward a convenient selection of landslide evaluative models (Nhu et al. 2020, Nhu et al. 2020, Panahi et al. 2020). In many works,

76 scholars have declared the better efficiency of soft computing models compared to traditional
77 statistical tools. Park et al. (2013) compared the performance of ANN with several FR, AHP, and LR
78 for landslide susceptibility mapping in Inje region, Korea. According to the respective values of area
79 under the curve (AUC) 0.789, 0.794, 0.794, and 0.806 obtained for the AHP, FR, LR, and ANN, the
80 superior accuracy of the ANN was deduced. A similar effort and conclusion were reported by Yilmaz
81 (2009) for a case study from Kat landslides in Tokat City of Turkey. Sadighi et al. (2020) showed the
82 ANFIS model outperforms ANN for landslide susceptibility modeling at Tajan Watershed, Northern
83 Iran. The AUC values were 0.902 and 0.866. However, a hybrid ANFIS (coupled with imperialist
84 competitive algorithm) with an AUC equal to 0.966 was found to be superior over both regular ANFIS
85 and ANN. Lucchese et al. (2021) employed and compared the ANN with ANFIS for the same purpose
86 in Rolante river basin, Brazil. Based on the calculated AUCs, 0.8886 for ANFIS and 0.9409 for ANN,
87 the later model could achieve a considerably larger accuracy.

88 The present research aims to produce applicable landslide susceptibility maps for the northern part of
89 Lecco Province, Italy. This country, owing to its relief and lithological and structural features, is
90 characterized by particularly high landslide risk (Trigila and Iadanza 2008). Having a look at the
91 existing literature, while some studies have dealt with landslide susceptibility prediction in different
92 parts of the Lombardy Region (Sterlacchini et al. 2011, Fabbri and Patera 2021), Lecco demands to
93 receive proper analysis for alleviating the risk of this catastrophe in this prone area.

94 Three different methodologies consisting of one traditional statistical method, namely frequency
95 ratio, and two artificial intelligence models, namely MLPNN and ANFIS, are employed in this
96 research to predict landslide susceptibility value (LSV) all over the area. The above studies have
97 professed the high efficiency of these three models (i.e., FR, ANN, and ANFIS) in the field of
98 landslide susceptibility assessment. In the following, the case study and used database are introduced
99 and spatial interactions are investigated. Then, the models are executed to produce and interpret the

susceptibility maps. It is followed by accuracy assessment along with comparative validation of the results, and finally, the study ends up with introducing a neural-based LSV predictive formula.

2 Data and case study

2.1 Study area

The case of this research is the Northern part of the Lecco province located in the Lombardy region, Italy. Figure 1 shows the exact location of the study area. It lies within the longitude 09º 15' to 09º 32' E and latitude 45º 50' to 46º 09' N adjacent to the Como Lake. The area is roughly 473 km^2 and referring to the 2007 census, the province of Lecco has nearly 340000 inhabitants (Parente et al. 2013). This region is under a warm and temperate climate with an annual rainfall around 1360 *mm*. According to online meteorological data (www.en.climate-data.org , www.worldweatheronline.com), the average monthly temperature ranges from 0 °C in January to 19.1 °C in August. The altitude varies from 197.3 *m* to 2608.6 *m*. The range of slope starts from 0 and peaks at around 87 ° close to the summits. According to the soil map, Cambisol is the dominant soil type covering around 45% of the area. Geologically, the area includes 43 units, out of which, the largest coverage is reported for Limestones and Dolomite. Considering the utilization of land, most of the area is classified as forest and semi-natural.

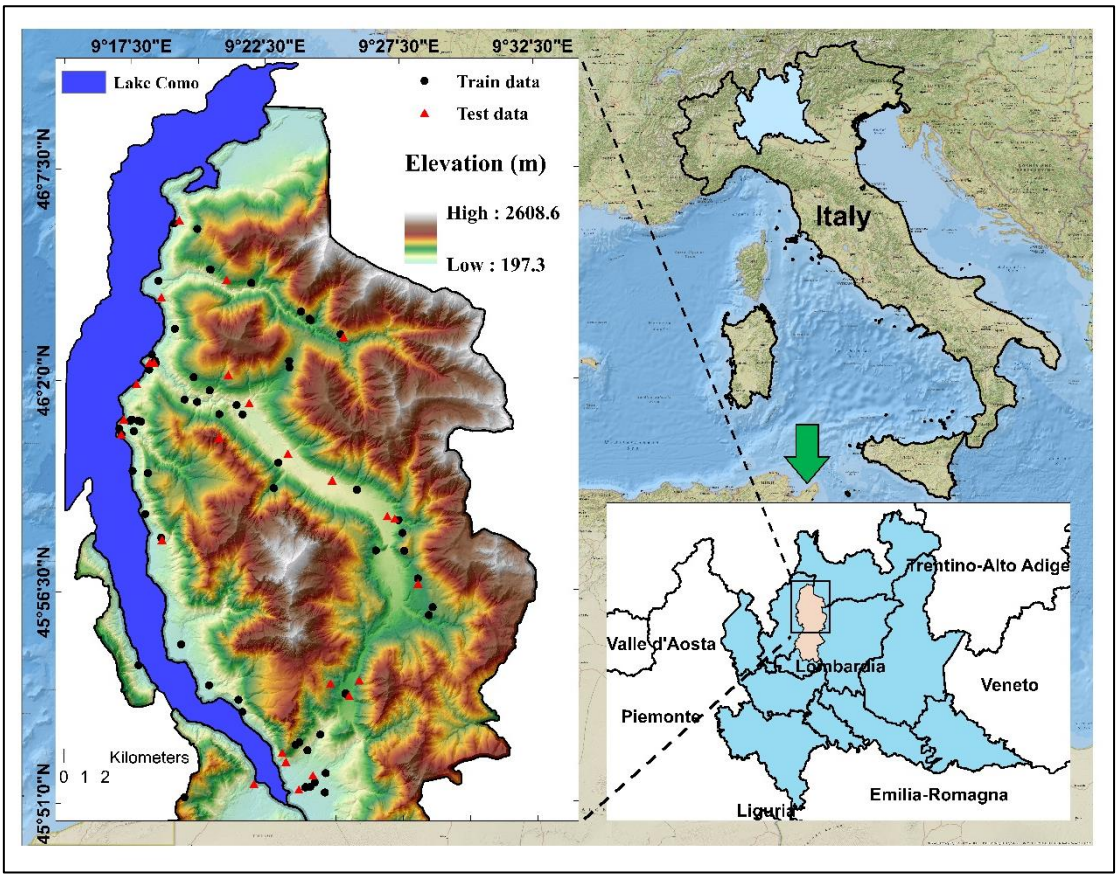

Figure 1: The study area and distribution of the landslides.

2.2 Landslide inventory map

Inventory maps are essential prerequisites for spatial analysis of environmental threats like landslides (Varnes 1984, Can et al. 2019). They illustrate the distribution of the past events within the area of interest, and contain also information regarding the date, outlines, and characteristics of occurrence (Singh and Kumar 2018, Chen et al. 2020). The inventory map used in this study merges the information of two published inventory maps. As Figure 1 shows, a total of 92 landslides are identified in the geographic information system (GIS). Out of these events, 82 landslides (18 areal + 64 single) are taken from the inventory map prepared by Calvello and Pecoraro (2018), and 10

128 landslides are taken from the database provided by the Inventario dei Fenomeni Franosi in Italia
129 (IFFI).

130 The landslides taken from the first dataset occurred between early-2010 and late-2019, while the
131 events taken from the IFFI dataset took place between 2000 and 2011. Considering the severity, the
132 landslides are mostly classified as C2: severe events with injured persons and/or evacuations, and C3:
133 minor events which did not cause any physical harm to people (Calvello and Pecoraro 2018).

134 To create the spatial database of this study, a total of 92 non-landslide points are randomly generated
135 within the areas without landslides. Based on a random selection, 70% of the landslides (i.e., 64
136 points) and 70% of the non-landslides (i.e., 64 points) are selected as training data, while the
137 remaining 30% (i.e., 28 landslides and 28 non-landslides) constitute the testing dataset.

138

139 **2.3 Conditioning factors and correlation assessment**

140 The susceptibility of landslide is a function of several parameters that can affect the occurrence of
141 this phenomenon. Therefore, proper selection of these parameters is of great importance (Dou et al.
142 2020, Li et al. 2021). Moreover, reliability of data is another key parameter as it contributes to the
143 quality of data (Mandal et al. 2021). In the present study, thirteen landslide conditioning factors,
144 namely elevation, slope aspect, slope degree, plan curvature, profile curvature, distance to waterway,
145 distance to road, distance to fault, soil type, land use, lithology, stream power index (SPI), and
146 topographic wetness index (TWI) are taken into the equation to predict the LSV. For preparing these
147 layers, the essential required layers were digital elevation model (DEM), the shapefile of linear
148 phenomena (i.e., waterways, roads, and faults), as well as the shapefiles of soil type, land use, and
149 geology map. All mentioned layers were downloaded from the website of Territorial Information of
150 Region Lombardy (Geoportal of the Lombardy Region:

(www.geoportale.regione.lombardia.it/en/home)) whose data is under either an IODL 2.0 or CC-BY-NC-SA 3.0 Italia license. The GIS layers were then clipped for the area of interest for data processing and subsequent analysis. According to the source metadata, the DEM layer has been provided with 5×5 *m* spatial resolution using various resources such as local topographical data, 1×1 *m* resolution Lidar surveys, and the former edition of the 20×20 *m* regional DEM (metadata).

Apart from the elevation layer that is represented by the DEM, the layers of slope aspect, slope degree, plan curvature, and profile curvature were directly produced from DEM. Figure 2 – (a) shows the elevation map. The altitude values range from 197.3 *m* to 2608.6 *m* which were classified into six groups including < 200, (200 - 700), (700 - 1200), (1200 - 1700), (1700 - 2200), and > 2200 *m*. The slope aspect, which illustrates the direction of slope face, has local influences on inducing instabilities of slopes (Chawla et al. 2019). Figure 2 – (b) shows the slope aspect. Based on the GIS classification, this layer has the following groups: Flat, North, North-East, East, South-East, South, South-West, West, and North-West. Famously, the slope is one of the most relevant factors in landslide susceptibility assessment which demonstrates the rate of change in altitude (Mathew et al. 2009, Mokarram and Zarei 2018). The produced slope map is presented in Figure 2 – (c). Based on this map, the gentlest and steepest terrains are represented by the slopes of 0° and 86.7°, respectively. This layer was classified into <15, (15 - 25), (25 - 35), (35 - 45), and > 45° (Tangestani 2009). Plan curvature is an indicator of flow acceleration and erosion/deposition rate and profile curvature can impact the variation of flow velocity down the slope (Kalantar et al. 2018, Moayedi et al. 2019). Figures 2 – (d) and (e) show the map of these two layers. The sub-classes of plan curvature were (-1897.01 - -59.10), (-59.10 - -22.34), (-22.34 - -10.09), (-10.09 - 51.16), and (51.16 - 1239.68), while the profile curvature consists of (-952.57 - -35.78), (-35.78 - -13.05), (-13.05 - -5.47), (-5.47 - 39.98), and (39.98 - 987.08) sub-classes.

Distance to linear features (i.e., waterways, road, and fault) has been among the most crucial conditioning factors for landslide susceptibility modeling that have been regarded in many previous efforts (Ozdemir and Altural 2013, Pradhan and Siddique 2020, Razavi-Termeh et al. 2021, Saha et al. 2021). Figures 2 – (f), (g), and (h) depict the maps of distance to waterways, distance to road, and distance to fault, respectively. The distribution of previous events indicates that the majority of landslides have occurred along with the named linear phenomena. The distance classes of (0 - 50), (50 - 100), (100 - 150), and >150 *m* were applied for the waterways and roads, while the map of distance to fault was grouped into (0 - 200), (200 - 400), (400 - 700), (700 - 1000), and >1000 *m* (Tangestani 2009).

Soil type is another important parameter that contributes to the occurrence of landslides through characteristics like permeability and cohesiveness (Avtar et al. 2011, Mandal et al. 2018). Seven soil categories are detected in the soil type map which is presented in Figure 2 – (i). These categories are originally Cambisols, Regosols, Fluvisols, Umbrisols, Cambisols podzolici, Leptosols, Luvisols that are represented by A, B, …, G in the corresponding map, respectively. The land use map was cropped from the CORINE Land Cover (CLC) layer. In the CLC legend, the utilizations are categorized into five major classes: (a) artificial surfaces, (b) agricultural areas, (c) forest and semi-natural areas, (d) water lands, and (e) water bodies. Each major class is further divided into two levels of classification. Consequently, a three-digit number indicates the land use of each sub-class (e.g., 312 stands for the land use category that is the 2nd sub-class belonging to the 1st class of the 3rd major category). More details regarding this layer can be found in (www.geoportale.regione.lombardia.it/en , www.land.copernicus.eu). Figure 2 – (j) displays the land use layer for the intended area. This map comprises 19 classes which are detailed in Table 1.

Table 1: The legend of the land use map (www.land.copernicus.eu).

CLC code	Name	Description	CLC code	Name	Description
312	A	Coniferous forests	324	K	Transitional woodland/shrub
231	B	Pastures	122	L	Road and rail networks and associated land
243	C	Principally agricultural with significant natural vegetation	121	M	Industrial or commercial units
313	D	Mixed forest	332	N	Bare rock
311	E	Broad-leaved forest	512	O	Water bodies
321	F	Natural grassland	242	P	Complex cultivation patterns
211	G	Non-irrigated arable land	131	Q	Mineral extraction sites
511	H	Water courses	333	R	Sparsely vegetated areas
112	I	Discontinuous urban fabric	111	S	Continuous urban fabric
322	J	Moors and heathland			

198

199 Lithology is a crucial parameter in landslide-related assessments as it can affect the formation and
200 evolution of landslides, as well as the type and scale of this phenomenon (Yalcin et al. 2011, Pham
201 et al. 2018, Xiao et al. 2019). Based on the lithology map (scale: 1:250000) shown in Figure 2 – (k),
202 a total of 43 geological units can be found in this area. As explained in Table 2, these layers are named
203 A, B, …, Z, AA, AB, … AQ.

204

205 Table 2: Description of the geological units.

Label	Original Description (In Italian)	Lithology
A	"Ortogneiss" e "Gneiss chiari" Auct.	Granitic and granodioritic Gneisses, Porphyroid
B	"Andesiti" ("Porfiriti" Auct.)	Andesites with Dacites, basalts, and Rhyolites
C	"Dolomia Principale"	Dolomites
D	anfiboliti (intercal.nei basam.cristallini)	Amphibolites
E	"Selcifero lombardo"	Flints Marl Limestone
F	Gneiss di Morbegno e altri	Paragneiss
G	marmi (intercal.nei basam.cristallini)	Marbles (crystalline Limestones)
H	morenico tardo-wurmiano e local. olocenico	Gravels, Blocks, Silts
I	"Verrucano lombardo"	Conglomerates, Sandstones
J	Cgl. del Ponteranica e del Dosso dei Galli	Conglomerates
K	conoidi	Conoids

L	Fmz. di Collio	Sandstones, Siltstones, Argillites
M	"Servino"	Sandstone, Marl, Siltstone, Argillite, Limestone; Siderite
N	"Micascisti dei Laghi"	Prevalent Mica Schists
O	"Dolomia a Conchodon"	Limestone and Dolomitic Limestone
P	Detriti di falda e frane	Groundwater debris and landslides
Q	Fmz. di Wengen/Fmz. di Buchenstein	Marl, Aren., calc., argil./calc. Sel., Aren., Marl, dol. S
R	"Rosso Ammonitico lombardo"/"Medolo"	Marls, Marly Limestones/Lombard Flint Limestones
S	Calcare di Prezzo/Calcare di Angolo	Limestones
T	Calcare di Esino e "Calcare rosso"	Limestones
U	Fmz. di San Giovanni Bianco	Argillites, Marls, Limestones, carnioles
V	Fmz. di Gorno	Limestone, Marl, sandstone, Argillite
W	Argillite di Riva di Solto	Shales
X	morenico Wurm	Gravels, Bubbles and Silts
Y	Calcare di Zu	Limestones
Z	Carniola di Bovegno	Carneole
AA	rioliti ("Porfidi quarziferi" Auct.)	Rhyolites + o - Alkal., Dacites and Subord. Trachytes and Latites
AB	dioriti e gabbri	Diorites and Gabri
AC	"Calcare metallifero bergamasco"	Limestones
AD	Sc.di Edolo/Fill.di Ambria/Micasc. di Maniv	Phyllites and Philladic Micascists "Quartz Phyllites" auct.
AE	Calcare di Camorelli	Limestones
AF	Dolomia dell'Albiga	Dolomites
AG	Calcare di Perledo-Varenna	Limestones
AH	Depositi terrazzati (Alluvium medio)	Gravels, Sands and Silts
AI	pegmatiti (intercal.nei basam.cristallini)	Pegmatites
AJ	Fmz. di Bellano	Conglomerates, Sandstones
AK	"Ceppo" e fmz. simili, facies "Villafran	Conglomerates, Sands, Clays
AL	Fluvioglaciale, fluviale e lacustre Riss	Ferrettized Gravels, Sands and Clays
AM	Arenaria di Val Sabbia	Sandstones
AN	Fluvioglaciale e Fluviale Wurm	Gravels, Sands
AO	Depositi terrazzati (Alluvium antico)	Gravels, Sands and Silts
AP	"Corna"	Limestones, Dolomites
AQ	"Scaglia lombarda"	Marl, Limestone Marn. Selcif Limestones. Basal tuff Sandstones.

206

207 The SPI and TWI are two important hydrological parameters that are frequently used in the landslide-
208 related analysis (Nsengiyumva et al. 2019, Saha and Saha 2021). The SPI denotes the erosive
209 potential of the streams (Kumar and Anbalagan 2016) and TWI is an indicator of soil moisture
210 contents that contribute to the occurrence of landslide (Pokharel et al. 2021). Given β as the steepness
211 of terrain and *SCA* as specific catchment area, Equations 1 and 2 express the formulation of these
212 conditioning factors:

$$SPI = SCA \times tan\beta \quad (1)$$

$$TWI = ln\,(SCA/tan\beta) \quad (2)$$

213 Figures 2 – (l) and (m) exhibit the maps produced for the SPI and TWI, respectively. The values of
214 both layers are classified into five classes. For the SPI the sub-groups are (0.01 - 1488.30), (1488.30
215 - 10418.13), (10418.13 - 32742.70), (32742.70 - 116087.75), and >116087.75. As for the TWI, (-9.62
216 - -2.66), (-2.66- 1.78), (1.78 - 3.72), (3.72 - 6.34), and >6.34.

217

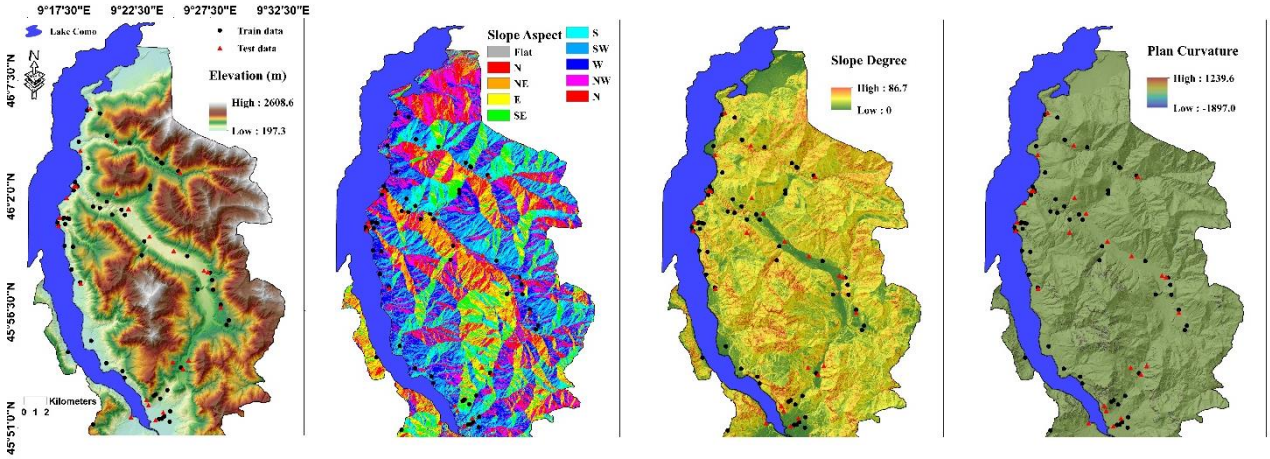

(a) (b) (c) (d)

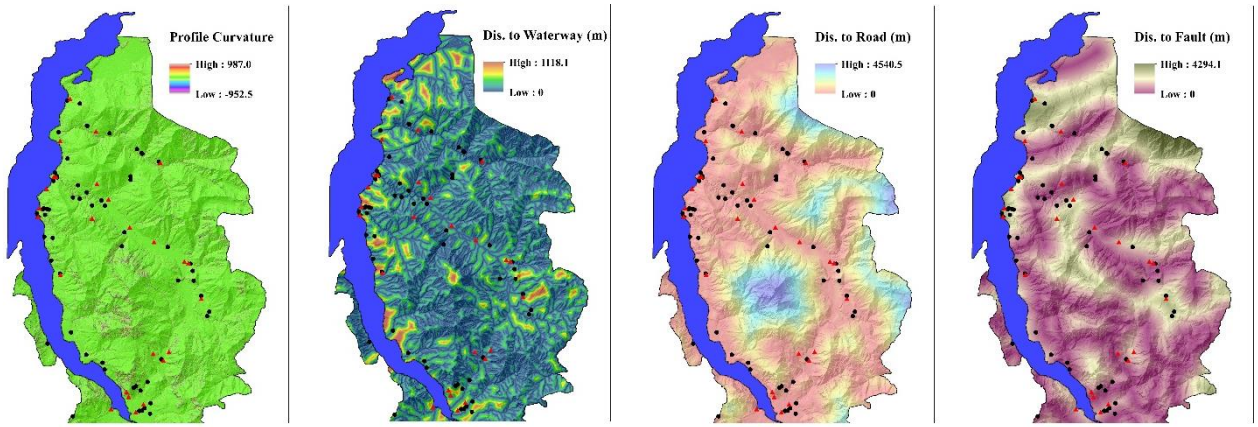

(e) (f) (g) (h)

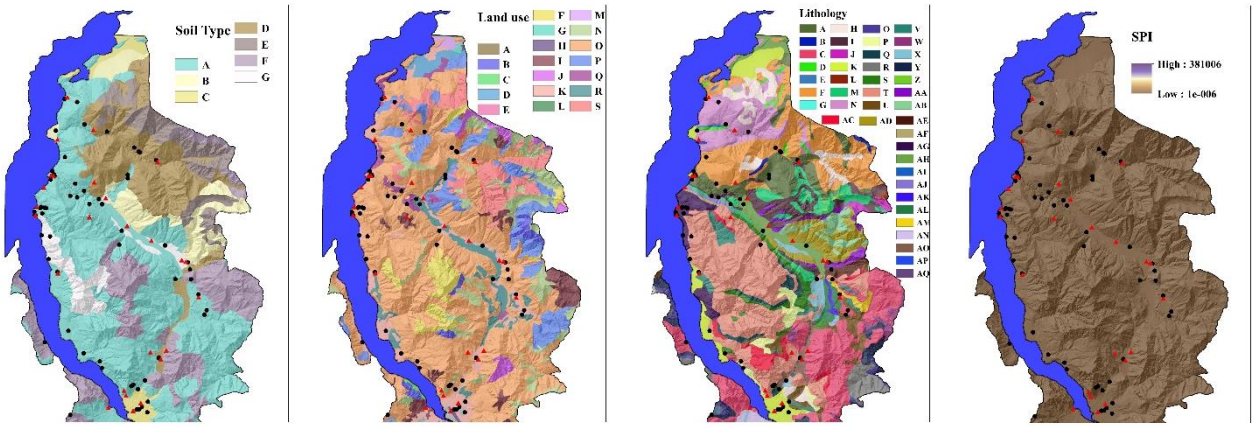

(i) (j) (k) (l)

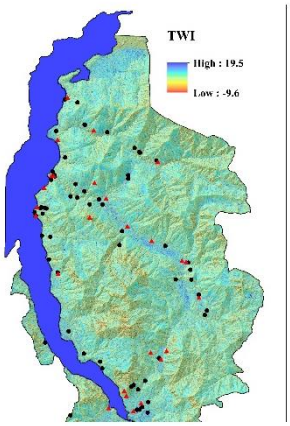

(m)

Figure 2: The map of conditioning factor: (a) elevation, (b) slope aspect, (c) slope degree, (d) plan curvature, (e) profile curvature, (f) distance to waterway, (g) distance to road, (h) distance to fault, (i) soil type, (j) land use, (k) lithology, (l) SPI, and (m) TWI

For quantifying the relationship between the landslides and conditioning factors, the FR model is employed. Since the FR is one of the models used in this study, it is well explained in the next section. In this method, based on statistical analysis, one value is calculated for each sub-class which determines its correlation with the landslide occurrence. Thus, the larger the FR is, the bigger the contribution of the sub-class is (Huang et al. 2021). Also, the FR values equal to 1 reflect an average

227 correlation, while those below 1 and above 1 indicate a lower and higher correlation (Akgün and
228 Bulut 2007).

229 All layers were prepared in the ArcMap with a cell size of 5×5 *m*. It resulted in layers with 18908558
230 pixels. The FR values were calculated by crossing each layer with the whole landslides. Table 3 gives
231 the results of this process. In the elevation map, the FR values of the first two classes are meaningfully
232 greater than others. In the aspect layer, the FR of South, South-West, and West is larger than 1.
233 Considering the slope map, around 43% of the landslides are located in slopes <15° which cover
234 approximately 14% of the area. It resulted in an FR value of 2.61. As for the plan curvature and profile
235 curvature layers, the biggest FRs (i.e., 2.44 and 2.64, respectively) are calculated for the fifth and first
236 sub-classes, respectively. Concerning the linear features, while large FRs are obtained for pixels far
237 from the waterway and faults, the pixels close to roads have significantly larger FRs. The biggest FR
238 in this regard is 6.03 for pixels which are at maximum 50 *m* off the roads. The sub-classes labeled as
239 C from the soil type layer, L from the land use layer, and AG from the lithology layer are characterized
240 by the largest correlation with the landslides. The smallest SPI sub-class and the largest TWI sub-
241 class acquired the highest FR which were 1.00 and 1.92, respectively.

242

243 Table 3: The details of conditioning factors and FR analysis.

Layer	Class	Number of Pixels	Percentage of Pixels	Number of Landslide Pixels	Percentage of Landslide Pixels	FR
Elevation (m)	< 200	103710	0.55	656	2.41	4.39
	(200 - 700)	5181809	27.40	18256	67.06	2.45
	(700 - 1200)	6739888	35.64	7995	29.37	0.82
	(1200 - 1700)	4830665	25.55	315	1.16	0.05
	(1700 - 2200)	1894308	10.02	0	0.00	0.00
	> 2200	158178	0.84	0	0.00	0.00
Slope Aspect	Flat	53802	0.28	31	0.11	0.40
	North	2276204	12.04	1647	6.05	0.50
	North-East	2025947	10.71	1785	6.56	0.61

	East	1618287	8.56	1344	4.94	0.58
	South-East	1807676	9.56	2243	8.24	0.86
	South	2387968	12.63	4101	15.07	1.19
	South-West	3016836	15.95	7917	29.08	1.82
	West	3057814	16.17	5081	18.67	1.15
	North-West	2664024	14.09	3073	11.29	0.80
Slope Degree	< 15	3101954	16.41	11641	42.76	2.61
	(15 - 25)	2997767	15.85	4841	17.78	1.12
	(25 - 35)	5316245	28.12	4669	17.15	0.61
	(35 - 45)	4997943	26.43	2977	10.94	0.41
	> 45	2494649	13.19	3094	11.37	0.86
Plan Curvature	(-1897.01 - -59.10)	40029	0.21	101	0.37	1.75
	(-59.10 - -22.34)	228573	1.21	543	1.99	1.65
	(-22.34 - -10.09)	557391	2.95	1067	3.92	1.33
	(-10.09 - 51.16)	18033856	95.37	25340	93.09	0.98
	(51.16 - 1239.68)	48709	0.26	171	0.63	2.44
Profile Curvature	(-952.57 - -35.78)	42953	0.23	163	0.60	2.64
	(-35.78 - -13.05)	249283	1.32	703	2.58	1.96
	(-13.05 - -5.47)	700050	3.70	1450	5.33	1.44
	(-5.47 - 39.98)	17879413	94.56	24805	91.12	0.96
	(39.98 - 987.08)	36859	0.19	101	0.37	1.90
Distance to Waterway (m)	(0 - 50)	6322640	33.44	7138	26.22	0.78
	(50 - 100)	4226169	22.35	5568	20.45	0.92
	(100 - 150)	2793515	14.77	3154	11.59	0.78
	> 150	5566234	29.44	11362	41.74	1.42
Distance to Road (m)	(0 - 50)	1799980	9.52	15634	57.43	6.03
	(50 - 100)	1290017	6.82	3831	14.07	2.06
	(100 - 150)	1033256	5.46	2458	9.03	1.65
	> 150	14785305	78.19	5299	19.47	0.25
Distance to Fault (m)	(0 - 200)	2847357	15.06	3436	12.62	0.84
	(200 - 400)	2620393	13.86	2851	10.47	0.76
	(400 - 700)	3341392	17.67	2758	10.13	0.57
	(700 - 1000)	2599794	13.75	5723	21.02	1.53
	> 1000	7499622	39.66	12454	45.75	1.15
Soil Type	A	8518775	45.05	14940	54.88	1.22
	B	1233376	6.52	776	2.85	0.44
	C	509657	2.70	2308	8.48	3.15
	D	3024208	15.99	3918	14.39	0.90
	E	1386236	7.33	0	0.00	0.00
	F	3414946	18.06	2052	7.54	0.42
	G	821360	4.34	3228	11.86	2.73
Land Use	A	1186813	6.28	37	0.14	0.02
	B	706696	3.74	1884	6.92	1.85
	C	252132	1.33	1189	4.37	3.28
	D	1726408	9.13	275	1.01	0.11
	E	9863373	52.16	9314	34.21	0.66
	F	1591860	8.42	630	2.31	0.27
	G	78409	0.41	212	0.78	1.88

	H	7747	0.04	0	0.00	0.00
	I	1033214	5.46	12210	44.85	8.21
	J	279027	1.48	0	0.00	0.00
	K	762117	4.03	315	1.16	0.29
	L	22735	0.12	315	1.16	9.62
	M	66065	0.35	0	0.00	0.00
	N	699371	3.70	0	0.00	0.00
	O	63175	0.33	810	2.98	8.91
	P	200116	1.06	0	0.00	0.00
	Q	43961	0.23	0	0.00	0.00
	R	242654	1.28	0	0.00	0.00
	S	82685	0.44	31	0.11	0.26
Lithology	A	925626	4.90	2249	8.26	1.69
	B	53518	0.28	0	0.00	0.00
	C	2485449	13.14	1796	6.60	0.50
	D	113803	0.60	102	0.37	0.62
	E	28220	0.15	0	0.00	0.00
	F	2146026	11.35	3182	11.69	1.03
	G	1525	0.01	0	0.00	0.00
	H	614398	3.25	0	0.00	0.00
	I	706462	3.74	1640	6.02	1.61
	J	80519	0.43	0	0.00	0.00
	K	717208	3.79	3429	12.60	3.32
	L	22197	0.12	0	0.00	0.00
	M	573513	3.03	36	0.13	0.04
	N	1142350	6.04	1874	6.88	1.14
	O	160430	0.85	0	0.00	0.00
	P	281857	1.49	595	2.19	1.47
	Q	214178	1.13	167	0.61	0.54
	R	388988	2.06	211	0.78	0.38
	S	341157	1.80	0	0.00	0.00
	T	3287997	17.39	3480	12.78	0.74
	U	420514	2.22	537	1.97	0.89
	V	283656	1.50	316	1.16	0.77
	W	185634	0.98	0	0.00	0.00
	X	257244	1.36	95	0.35	0.26
	Y	386464	2.04	99	0.36	0.18
	Z	20293	0.11	0	0.00	0.00
	AA	215974	1.14	294	1.08	0.95
	AB	298637	1.58	0	0.00	0.00
	AC	310488	1.64	0	0.00	0.00
	AD	609699	3.22	875	3.21	1.00
	AE	115341	0.61	0	0.00	0.00
	AF	26950	0.14	9	0.03	0.23
	AG	362033	1.91	2846	10.45	5.46
	AH	471572	2.49	1554	5.71	2.29
	AI	10603	0.06	0	0.00	0.00
	AJ	47214	0.25	215	0.79	3.16

	AK	42261	0.22	0	0.00	0.00
	AL	135095	0.71	170	0.62	0.87
	AM	84775	0.45	0	0.00	0.00
	AN	136238	0.72	217	0.80	1.11
	AO	198793	1.05	1234	4.53	4.31
	AP	2545	0.01	0	0.00	0.00
	AQ	1114	0.01	0	0.00	0.00
SPI	(0.01 - 1488.30)	18785148	99.35	27122	99.63	1.00
	(1488.30 - 10418.13)	110058	0.58	97	0.36	0.61
	(10418.13 - 32742.70)	12295	0.07	3	0.01	0.17
	(32742.70 - 116087.75)	1036	0.01	0	0.00	0.00
	> 116087.75	21	0.00	0	0.00	0.00
TWI	(-9.62 - -2.66)	1901680	10.06	4241	15.58	1.55
	(-2.66- 1.78)	4226507	22.35	5461	20.06	0.90
	(1.78 - 3.72)	7672662	40.58	7870	28.91	0.71
	(3.72 - 6.34)	4158012	21.99	7031	25.83	1.17
	> 6.34	949697	5.02	2619	9.62	1.92

3 Methodology

The strategy taken for fulfilling this objective is depicted in Figure 3. After proper provision of landslide conditioning factors and inventory map, the FR model delineates the spatial correlation between the landlised and conditioning factors. The database is then divided into the training and testing subsets. Utilizing the training set, the FR, MLPNN, and ANFIS models are executed to calculate landslide susceptibility values (LSVs) over the study area in order to produce the susceptibility maps. The accuracy of the produced maps is evaluated with the help of testing points. Following this, a comparison points out the most accurate evaluative model. Finally, an explicit formula is derived from the MLPNN model to be used for conveniently approximating the LSV.

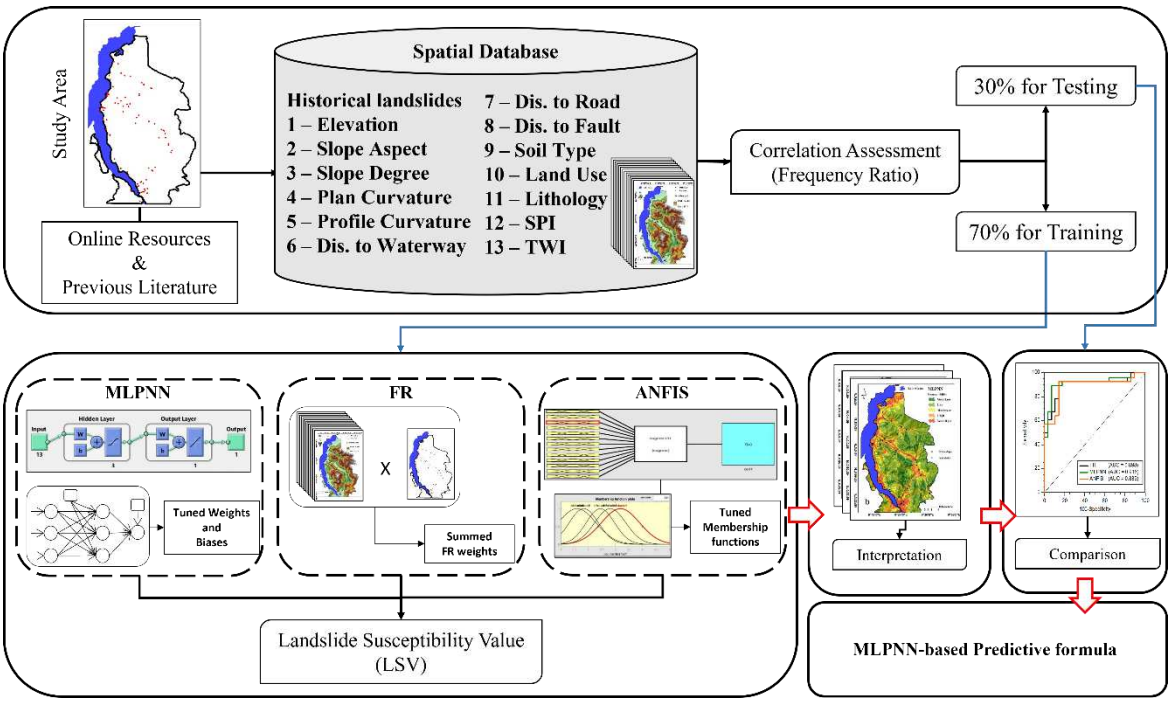

Figure 3: The graphical methodology of this research.

The mechanism of the employed models (i.e., FR, MLPNN, and ANFIS) is explained in the following.

3.1 Frequency Ratio

The FR model is a simple bivariate statistical approach that enables the user to acquire a quantitative representation from the spatial relationship between the landslide and conditioning factors (Termeh et al. 2018). It is a broadly used tool for probabilistic assessments of natural hazards in which multi-classified maps are involved (Bonham-Carter 1994).

In the FR method, each sub-class is distinguished by a weight, for calculating which, two questions should be regarded. Assuming the landslide susceptibility problem, the questions are: (a) what

percentage of landslide pixels are included in this sub-class? and (b) what percentage of the whole area does this sub-class cover? Equation 3 can be written as follows:

$$FR = \frac{l/L}{a/A} \tag{3}$$

in which l represent the number of landslide pixels included in the sub-class of interest, L is the number of all landslide pixels, a symbolizes the number of pixels corresponding to the sub-class of interest, and A is the number of pixels all over the study area. The LSV of each pixel is finally calculated by summing the FR values obtained for all conditioning factors.

3.2 MLPNN

An MLPNN is a specific powerful type of ANNs that is distinguished by its layered structure (Hornik 1991). Generally speaking, ANNs are deemed as simulated biological neural networks which are capable of exploring complex engineering problems (Hornik et al. 1989, Seyedashraf et al. 2018). Provided a numerical dataset, the network uses part of the data for pattern recognition (i.e., training) and the rest is exposed to the obtained knowledge as testing data. Since the model has not met with the testing data before, the testing performance can represent the generalization power of the model. The components of an MLPNN are neurons (A.K.A nodes) that are connected by synapses. As Figure 4 depicts the MLPNN used in this study, the connection is handled by weights (black arrows). These weights, as well as some bias terms (blue arrows), are tunable through the training process.

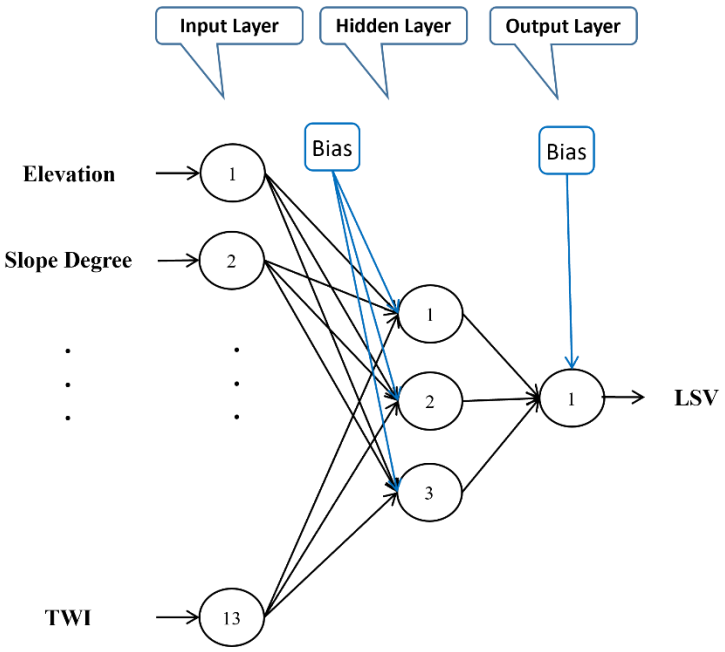

Figure 4: The structure of the used MLPNN.

Utilizing specific training strategies (e.g., backpropagation technique associated with the Levenberg-Marquardt algorithm (Moré 1978)) the neurons perform calculations in the form of Equation 4 to establish a non-linear dependency between the LSV and conditioning factors.

$$Output = g(W \times CF + b) \quad (4)$$

where W and b signify the involved weight and bias, respectively. Also, CF is the conditioning factor and $g()$ represents the activation function of the neuron.

3.3 ANFIS

An ANFIS is a hybrid tool composed of the intelligent computational strategy of the ANN and fuzzy logic. This model was designed by Jang (1993). Taking the advantage of if-then rules with respect to human experience, fuzzy logic attempts to map non-linear complexities into scalar formats. The

calculations in a fuzzy-based model draw on three major processors, namely fuzzification, a fuzzy inference engine, and defuzzification. Based on this idea, crisp values are transformed into a linguistic fuzzy variable for feeding a FIS. The FIS then uses implication operations to apply so-called elements "fuzzy rules" to fuzzy variables. Lastly, the outcome of this process is converted into crisp format again (i.e., defuzzification procedure) (Alajmi and Almeshal 2020). Equivalent to the weights and biases in an ANN, the parameters of the fuzzy membership functions are tunable items in the ANFIS.

3.4 Accuracy indicators

Plotting the receiving operating characteristic (ROC) curve, along with computing the area beneath it, i.e., the AUC index, is a recognized accuracy evaluation approach in such studies (Zabihi et al. 2018, Moayedi et al. 2019, Nguyen et al. 2019, Jiang et al. 2021). The ROC diagram draws specificity on the *x*-axis versus sensitivity on the *y*-axis. Sensitivity denotes the proportion of correctly classified landslide pixels, while specificity is expressed as the proportion of correctly classified non-landslide pixels. Having TP, TN, FP, and FN as true positive, true negative, false positive, and false negative, respectively, specificity and sensitivity are calculated as follows (Chen et al. 2017, Hong, Liu et al. 2018):

$$Sensitivity = \frac{TP}{TP + FN} \tag{5}$$

$$Specificity = \frac{TN}{FP + TN} \tag{6}$$

Note that the TP and TN stand for the numbers of correctly classified pixels, whereas FP and FN signify the numbers of erroneously classified pixels.

Moreover, two error indicators, namely mean square error (MSE) and mean absolute error (MAE) are used to calculate the error of prediction. Let $LSV_{i_{expected}}$ and $LSV_{i_{modelled}}$ represent the real (i.e., 0 and 1) and predicted LSVs, respectively, the MSE and MAE are defined as follows:

$$MSE = \frac{1}{Z}\sum_{i=1}^{Z}(LSV_{i_{expected}} - LSV_{i_{modelled}})^2 \quad (7)$$

$$MAE = \frac{1}{Z}\sum_{i=1}^{Z}\left|LSV_{i_{expected}} - LSV_{i_{modelled}}\right| \quad (8)$$

in which the number of landslide points is represented by Z (which equals 128 for the training dataset and 56 for the testing dataset).

4 Results

To fulfill the purpose of the study, statistical and intelligent models are used to analyze the relationship between the landslide and its conditioning factors, and subsequently, predict the susceptibility for the area of interest. The results of the research are presented in this section. First, an importance analysis is carried out to evaluate the contribution of each conditioning factor. Next, the implementation of the models is explained, and after producing the landslide susceptibility maps, the accuracy of the models is assessed and compared.

4.1 Importance analysis

The importance of each landslide conditioning factor is investigated using an unbiased predictor importance approach. In this regard, a random forest (RF), i.e., a bagged ensemble, composed of 200 regression trees is trained in the Matlab environment (Zheng et al. 2020, Moayedi et al. 2021). Figure

5 shows the obtained importance values (IVs) in the form of column charts. It is clearly seen that distance to road (IV = 2.62) plays the most important role in this dataset. After that, elevation (IV = 2.62), slope degree (IV = 0.41), and slope aspect (IV = 0.38) have the largest contributions.

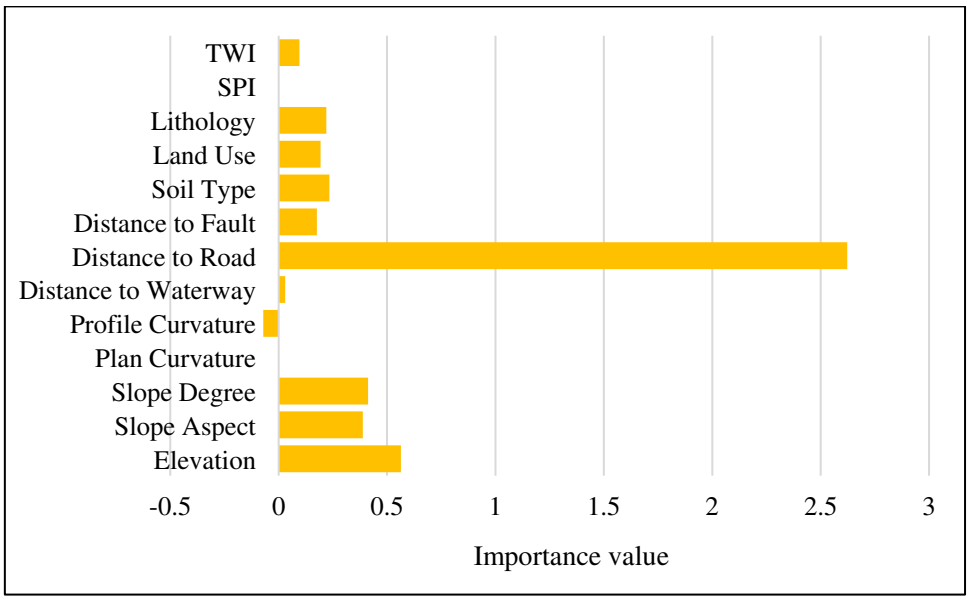

Figure 5: The results of the importance assessment.

4.2 Model implementation

For all three models, the training data are used for acquiring the knowledge regarding the landslide pattern and the susceptibility maps are produced accordingly. More clearly, based on the existing events, the model conducts specific calculations to explore the landslide pattern and applies this knowledge to the whole area for producing the landslide susceptibility map.

4.2.1 FR

For producing the landslide susceptibility map using FR, the training events were crossed with the classified map of the conditioning factor to calculate the $^{l}/_{L}$ and $^{a}/_{A}$ ratios (see Equation 3).. After calculating the FR value for each sub-class, the susceptibility map was obtained as the sum of all weight layers. It is worth noting that the FR values used for producing this map were different from those presented in Table 3 as the values in this table are calculated when all landslides are concerned.

4.2.2 Artificial intelligence models

Implementing intelligent models like the MLPNN and ANFIS entails providing appropriate numerical data to feed their networks. The values of thirteen conditioning factors were extracted to a total of 184 points (having 92 landslides and 92 non-landslides). Moreover, each point received a target value which was either 0 or 1 if it is a non-landslide or landslide point, respectively. After separating the 56 testing points, a training dataset composed of 128 samples was provided for the MLPNN and ANFIS. They explore this dataset to acquire a non-linear understanding of landslide susceptibility.

4.2.2.1 MLPNN

Due to the number of inputs (i.e., 13) and the unique target parameter, it is immediate that the proposed MLPNN should have 13 input neurons and one output neuron. In contrast, determining the number of hidden neurons is a challenging task in ANN models. Trial and effort, coupled with the user's experience, is a well-tried approach for properly determining this parameter. In this study, 50 MLPNNs with the architecture $13 \times x \times 1$ (x = 1, 2, 3, …, 50) were considered where each one was

executed 5 times for assessing the repeatability of results. This process revealed that 3 hidden neurons give the best results. Hence, an MLPNNs with the architecture 13 × 3 × 1 was chosen among a total of 250 tested networks. This model was trained by Levenberg-Marquardt (LM) algorithm (Marquardt 1963) which is among the most powerful techniques for this objective. In the training process, based on the influence of conditioning factors on the occurrence of landslides, the weights and biases of the MLPNN were adjusted. Almost in all cases, the divergence of the error (with 6 times tolerance) stopped the training process.

Figure 6 shows the training results. In this figure, the predicted LSVs are compared to the expected ones (i.e., 0 and 1). For each sample, an error value gives the direct difference between these two values, and the frequency of these errors is analyzed in the form of a histogram chart. The calculated values of MSE (0.1115) and MAE (0.2623) associated with this graphical representation indicate acceptable learning carried out by this model.

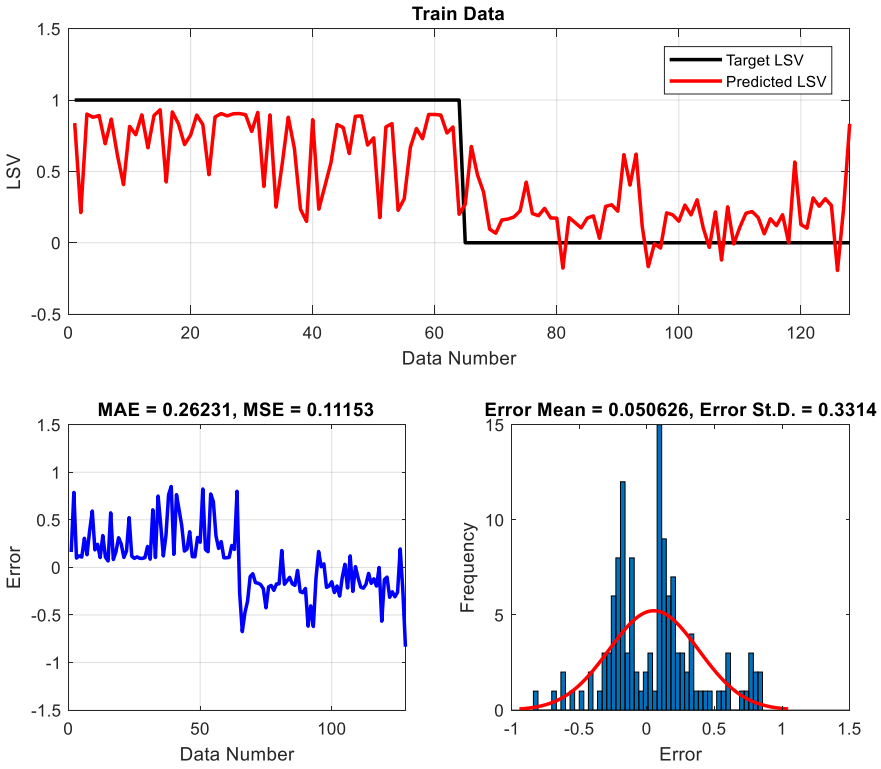

Figure 6: Training results of the MLPNN model.

4.2.2.2 ANFIS

Similar to the MLPNN, there are some parameters that should be determined for achieving a reliable implementation of the ANFIS. The number of clusters in a fuzzy inference system can significantly affect the quality of learning. This parameter was tested to be 4, 5, 6, 7, and 8 (the values outside this range did not yield reasonable training). Each model was repeated 10 times to check the repeatability of results. Finally, out of 50 tested models, the ANFIS with 6 clusters was chosen due to the lowest training error provided by this architecture. Concerning other parameters of the ANFIS, the number of repetitions (i.e., epochs) was set to be 1000. A few greater values were tested as well, but the network experienced negligible changes. Between the Hybrid and Backpropagation optimization methods, the latter method was preferred based on a trial-and-error effort.

Figure 7 exhibits the training performance of the ANFIS. As is seen, the network has acquired a good understanding of the behavior of landslides. The responses of the network corresponding to the landslide data tend to 1, and likewise, those corresponding to the non-landslide data tend to 0. Based on the MAE and MSE values equaling 0.2278 and 0.0932, respectively, the training error is in an acceptable range. These errors are also smaller than the MLPNN model.

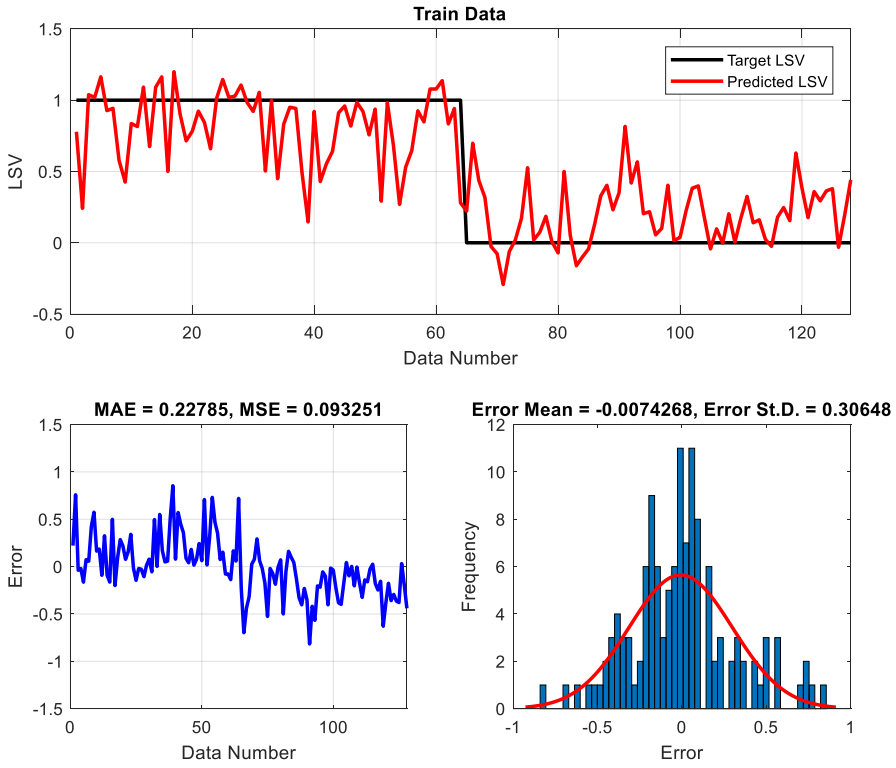

Figure 7: Training results of the ANFIS model.

4.3 Susceptibility maps and interpretation

Three landslide susceptibility maps are prepared. As explained, the calculations of the FR model were carried out in the ArcGIS and the map was obtained after statistically analyzing spatial interactions. The procedure for producing the susceptibility maps of the MLPNN and ANFIS was different. For all pixels, the values corresponding to thirteen conditioning factors were converted to ASCII format. Then, they were given to the trained networks of MLPNN and ANFIS as new environmental conditions. The models predicted an LSV for each pixel and the results were imported back into ArcGIS to produce the susceptibility maps.

The next step was classification of the maps to propose susceptibility levels within the studied area. To this end, the Natural Break classification technique was applied and yielded five categories

characterizing very low, low, moderate, high, and very high susceptibility. It is worth mentioning that the Natural Break (A.K.A Jenks optimization method) is a well-tried classifier for the maps of natural hazards and phenomena (Pourtaghi et al. 2015, Tehrany et al. 2019). For a certain number of classes, it aims to detect breaks that maximize between-class differences and minimizes within-class variance (Ahmed et al. 2021).

Figure 8 – (a), (b), and (c) present the resulted maps. It can be seen that these maps are of good reliability, due to compatibility with the occurred landslides. The location of many previous events has been characterized by high or very high susceptibility. An appreciable point deduced from these maps is the high susceptibility of the northern part of the case study (around the road network) where no landslide has been reported. In contrast, some vast central and eastern regions are represented by green colors exhibiting low susceptibility.

To have a better perception of the susceptibility areas, Figure 8 – (d) shows the places showing very high susceptibility jointly by the FR, MLPNN, and ANFIS models. According to this map, as well as the 3D view shown in Figure 8 – (e), a significant part of the coastline of Lake Como (Lecco side) is deemed as crucially susceptible. For instance, a view of the municipality of Bellano is shown in Figure 8 – (f) using Google Earth photos. As the yellow marks are seen on the map, this area has before experienced several landslides.

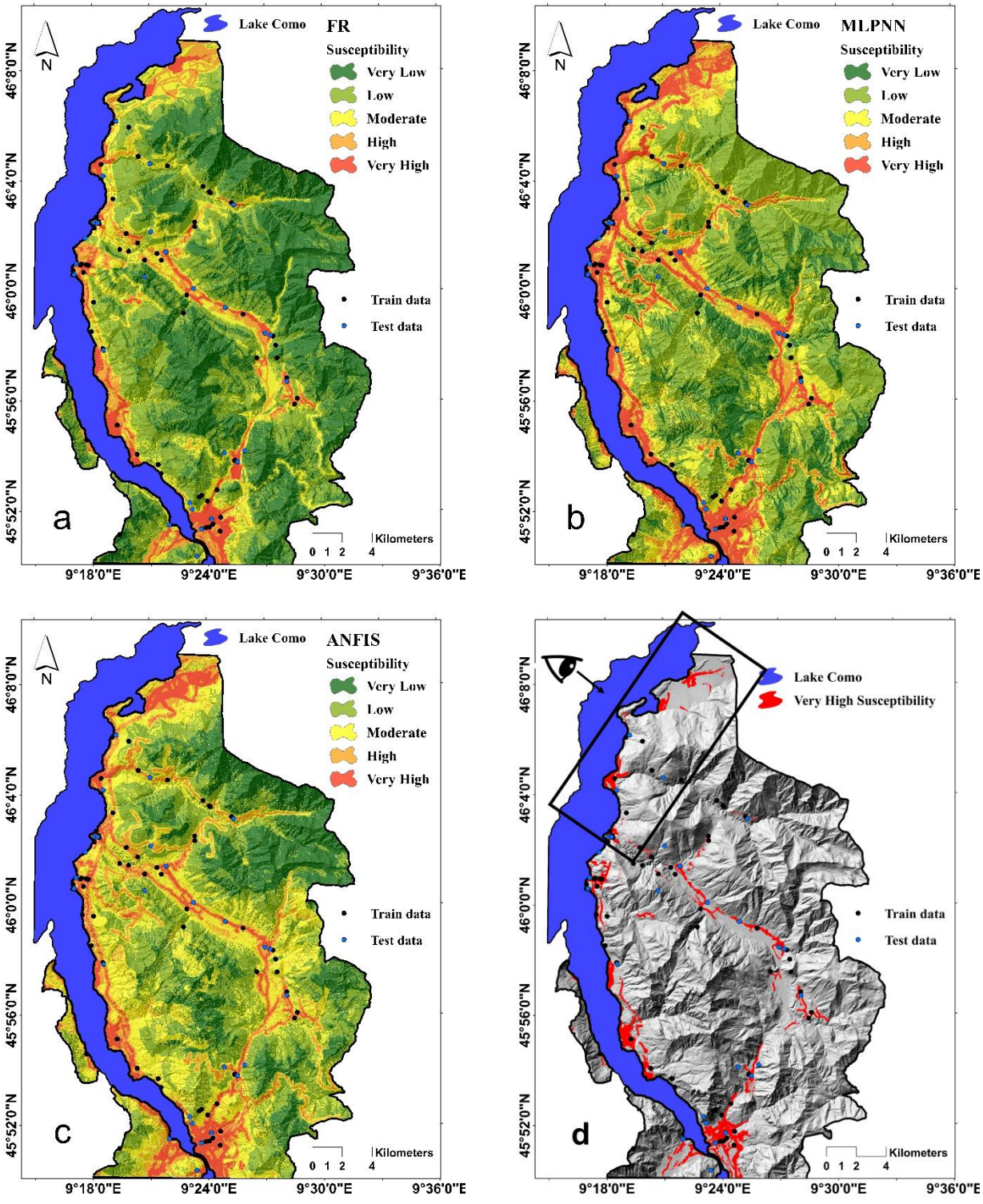
Lake Como
FR
Susceptibility
Very Low
Low
Moderate
High
Very High
Train data
Test data
a
Kilometers
0 1 2 4
N
46°8'0"N
46°4'0"N
46°0'0"N
45°56'0"N
45°52'0"N
9°18'0"E
9°24'0"E
9°30'0"E
9°36'0"E
Lake Como
MLPNN
Susceptibility
Very Low
Low
Moderate
High
Very High
Train data
Test data
b
Kilometers
0 1 2 4
Lake Como
ANFIS
Susceptibility
Very Low
Low
Moderate
High
Very High
Train data
Test data
c
Kilometers
0 1 2 4
Lake Como
Very High Susceptibility
Train data
Test data
d
Kilometers
0 1 2 4

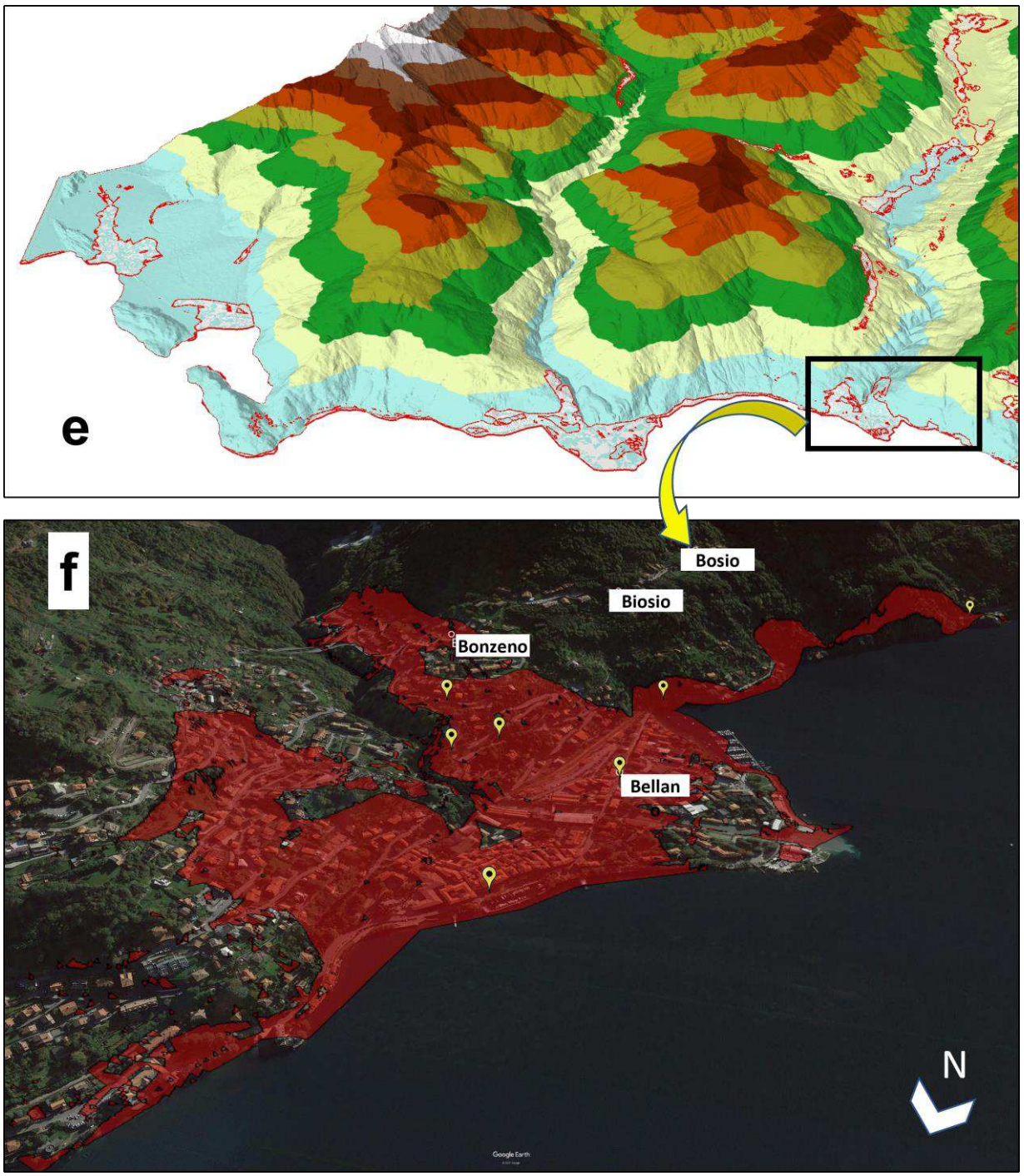

433 Figure 8: The landslide susceptibility maps produced by (a) FR, (b) MLPNN, and (c), ANFIS, (d)
434 very high susceptible areas identified by all three models, (e) a 3D view of Northern parts, and (d) a
435 Google Earth view detailing the susceptibility of the municipality of Bellano.

436

Another susceptible line is in the low-height central area. In accordance with the map of conditioning factors, these areas are mostly overlaid with the road networks. The high contribution of the road networks was also inferred from the importance assessment (see Figure 5) where the greatest importance was obtained for the factor distance to road. It necessitates applying proper mitigation measures along the main roads.

A notable discrepancy with the expectation is the high susceptibility of gentle terrains. Crossing Figure 8 – (d) with the classified slope map revealed that the slope corresponding to 81.41% of the susceptible areas is below 15°. This observation can also be supported by the FR analysis (see Table 3) where the biggest FR was observed for this group (<15°) of slope layer. Hence, the areas with gentle slopes may receive equal, and even higher attention, compared to steep areas.

The same procedure was repeated for the layers of land use, soil type, and lithology. Areas distinguished with land use code 112 (i.e., discontinuous urban fabric with largest FR = 8.21) have around 77.5% overlay with Figure 8 – (d). Likewise, Cambisols and Fluvisols are soil types that contain around half and one-fourth of the crucially susceptible areas, respectively. Concerning the geological units, approximately 40% of Figure 8 – (d) falls into the K-labeled unit (i.e., Conoids) having an FR value of 3.32.

Table 4 reports the percentage of the area that is covered by each susceptibility class. According to this report, the majority of the area has been categorized as low and very low susceptible. The FR, MLP, and ANFIS have determined 5.03%, 12.6%, and 8.12% of the area as very high susceptible, respectively. Table 4 also demonstrates the percentage of training and testing landslides found in each susceptibility class. Around 45%, 66%, and 55% of the training points, and around 54%, 68%, and 57% of the testing point are estimated (respectively by the FR, MLPNN, and ANFIS), to be in areas under very high susceptibility.

Table 4: Areal percentage of susceptibility class and intersection with training and testing points.

Susceptibility Class	FR			MLPNN			ANFIS		
	Area	Training points	Testing points	Area	Training points	Testing points	Area	Training points	Testing points
Very Low	38.48	1.56	7.14	13.81	1.56	0	19.68	0	3.57
Low	36.22	14.06	0	44.94	9.37	7.14	33.09	6.25	3.57
Moderate	12.62	7.81	25	18.28	9.37	0	26.15	12.5	0
High	7.62	31.25	14.28	10.35	14.06	25	12.94	26.56	35.71
Very High	5.03	45.31	53.57	12.6	65.62	67.85	8.12	54.68	57.14

4.4 Validation and comparison

The landslide points that were selected as the testing data were used to examine the accuracy of the maps. It was explained that this study employs the AUC as a common accuracy indicator for all three models. Figure 9 depicts the ROC diagram obtained for the prediction of the FR, MLPNN, and ANFIS. Having a glance at this diagram, all three models have produced susceptibility maps with reliable accuracy. Based on the calculated AUC values, the line corresponding to the MLPNN has the largest area underneath. With 91.6% accuracy, the MLPNN was the most accurate model, followed by the FR and ANFIS with 89.8% and 88.9% accuracy, respectively.

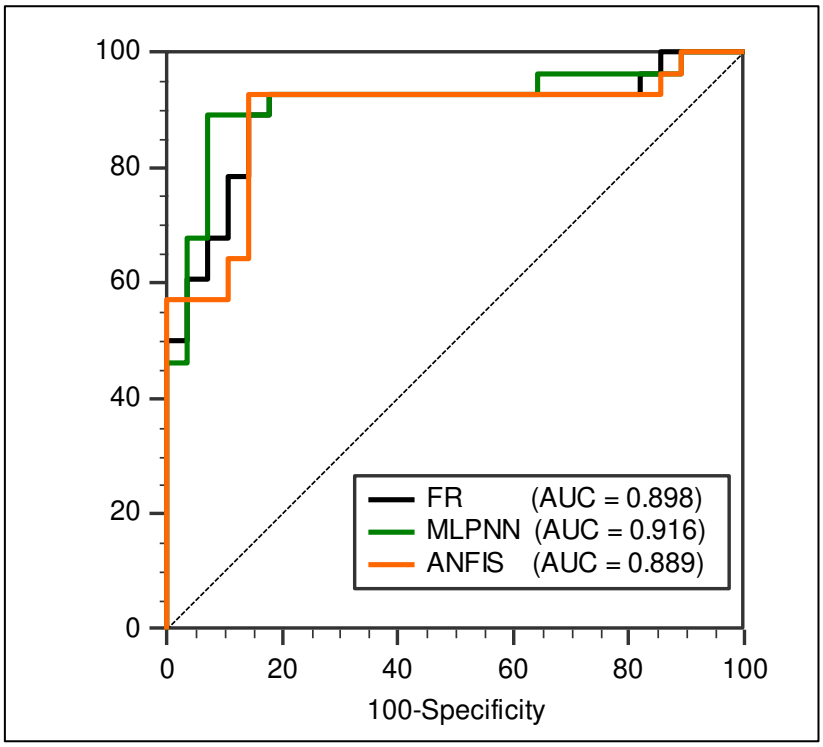

Figure 9: Comparison of the ROC curves.

The results of the models are also compared in terms of sensitivity, specificity, and standard error. The sensitivity and specificity of a model indicate true positive and false negative rates in assessing the classification accuracy, which in this case respectively correspond to classifying the landslide and non-landslide points (Bui et al. 2020). With 92.86% sensitivity, the performance of the FR and ANFIS was superior to MLPNN (sensitivity = 89.29%) in the classification of landslides, while the MLPNN, concerning a specificity value of 92.86%, performed the best in the classification of non-landslide points. The calculated specificity values for the FR and ANFIS were 82.14% and 85.71%, respectively. Furthermore, the lowest standard error was reported for the MLPNN, i.e., 0.0428 vs. 0.0464 for the FR and 0.0489 for the ANFIS.

Referring to the above comparison of the accuracies of classification, the MLPNN could predict the susceptibility of landslide more successfully than the FR and ANFIS. Here, two intelligent models

(i.e., the MLPNN and ANFIS) are also compared in terms of the MSE and MAE which reflect error of prediction. The MSE and MAE of the ANFIS were 0.1425 and 0.2939, while these values were 0.1139 and 0.2720 for the MLPNN. Both criteria demonstrate that the neural model was stronger for predicting the landslide pattern in unseen environmental conditions.

4.5 An explicit LSV formula

In section 3.2, the prediction strategy of the MLPNN was mathematically described. Therefore, after training the model, its neural configuration exposes an explicit predictive formula that can be used for predicting the LSV. The MLPNN was structured as $13 \times 3 \times 1$ denoting 13 input neurons, 3 hidden neurons, and 1 output neuron. Accordingly, there are $(13 \times 3 =)$ 39 weights that connect the input and hidden neurons and $(3 \times 1 =)$ 3 weights that connect the hidden and output neurons (see Figure 4). Also, each of the hidden and output neurons owns a bias term for creating their equations. Altogether, the formula is composed of 46 parameters. Equation 9 expresses the LSV formula wherein distance to waterway, distance to road, and distance to fault are abbreviated as DTW, DTR, and DTF, respectively.

$$\begin{aligned} LSV = {} & 0.235355754897564 \times (Tansig\,(0.49611697103011 \times DTW - 0.28215975145404 \times DTR + 0.10519510174892 \times DTF - \\ & 0.03948908963709 \times Plan\ Curvature - 0.71556154329431 \times Profile\ Curvature - 0.06841561591420 \times SPI - 0.20196853262512 \times \\ & TWI + 0.56168659367406 \times Slope + 0.73046437373474 \times Elevation - 0.13523545965545 \times Aspect + 0.39110715875350 \times Soil \\ & Type + 0.43253792274473 \times Land\ Use + 0.46099265923345 \times Lithology - 1.52939635508597)) + 0.742241903694308 \times (Tansig \\ & (0.03077577233479 \times DTW - 0.74638631888807 \times DTR + 0.19058068938466 \times DTF - 0.04668454023551 \times Plan\ Curvature - \\ & 0.72881353591087 \times Profile\ Curvature - 0.13035446606329 \times SPI + 0.04891053458325 \times TWI - 0.41063937103937 \times Slope - \\ & 1.23802118690475 \times Elevation - 0.12289902151882 \times Aspect - 0.01460096443284 \times Soil\ Type + 0.46066208565070 \times Land\ Use \\ & + 0.26589888120670 \times Lithology - 0.02994344768701)) - 0.440372657429712 \times (Tansig\,(-0.44020371440657 \times DTW + \\ & 0.38506975471705 \times DTR - 0.58073685920043 \times DTF + 0.89447215261175 \times Plan\ Curvature + 0.56358583423041 \times Profile \\ & Curvature + 0.34525011109460 \times SPI + 0.59765726539481 \times TWI - 0.15203094699963 \times Slope + 0.23360725777276 \times Elevation \\ & - 0.83846450148649 \times Aspect - 0.40035536706221 \times Soil\ Type + 0.26889703594242 \times Land\ Use + 0.46829096733901 \times Lithology \\ & - 1.41416958693356)) - 0.10370417873949 \end{aligned} \tag{9}$$

where *Tansig()* is the activation function that is employed by the hidden neurons for producing the local outputs (*g()* in Equation 4). This function is expressed by Equation 10.

$$Tansig\ (x) = \frac{2}{1 + e^{-2x}} - 1 \tag{10}$$

5 Discussion

5.1 Problem and solution

Susceptibility prediction is an effective solution for dealing with environmental threats (Sun et al. 2020, Wei et al. 2021). In the case of landslides, prediction-oriented efforts are of great value to engineers and decision-makers toward providing appropriate mitigation measures and land use planning (Ngo et al. 2021). Up to now, a wide variety of modeling tools and strategies have been proposed to model the susceptibility of landslide all over the world. Concerning the methodologies that require prior landslide events as primary information, statistical-based model and artificial intelligence are among the most popular ones.

This study employed the FR and two intelligent models (i.e., MLPNN and ANFIS) for landslide susceptibility prediction in the province of Lecco (Northern half). Using high-resolution data led to producing detailed landslide susceptibility maps. Moreover, accuracy assessments revealed that all three maps can yield a reliable approximation of the susceptible areas. The AUC values corresponding to the prediction phase were 0.898, 0.916, and 0.889 that profess high robustness of all three models against the complexity and non-linearity of the given problem.

5.2 A comparative evaluation

From a comparative viewpoint, spatial assessments using bivariate statistical approaches (e.g., FR) are associated with disadvantages like being time-consuming (Yilmaz 2010) and disregarding the interaction between variables (in determining the weight) (Ozdemir 2011). This is while both of these weaknesses are nicely overcome when artificial intelligence techniques are applied. They are capable of automatically tunning the variables in a very efficient way. Nonetheless, a significant difficulty in using intelligent models lies in the necessity of converting the GIS data into pure numerical formats like ASCII. Choosing appropriate hyperparameters is another issue that should be carefully taken care of (Youssef and Pourghasemi 2021). Determining the number of hidden neurons in MLPNN (or the number of clusters in ANFIS) is an example of this challenge that, in the present research, was solved by taking the advantage of the trial-and-error method.

Both MLPNN and ANFIS were trained using the backpropagation strategy in which the algorithm propagates backward for rectifying the parameters with respect to the calculated error. The backpropagation is a capable landslide evaluative model which has been successfully tried by scholars like Pradhan and Lee (2010) and Wu et al. (2013). Although the ANFIS achieved a more accurate training (MSEs of 0.0932 vs. 0.1115), the testing performance of the ANN was superior (MSEs of 0.1139 vs. 0.1425). It can reflect the higher flexibility of the MLPNN when it is applied to unseen environmental conditions. Altogether, the MLPNN was introduced as the most efficient landslide evaluative model, based on which, an explicit LSV predictive formula was extracted.

5.3 Comparison with literature

Based on the provided inventory maps, landslide is considered a frequent major natural disaster in Italy (Trigila et al. 2010). The produced susceptibility maps were in complete agreement with

historical landslide events of the Lecco Province. Nonetheless, the outcomes are compared with the results of earlier studies conducted for different scales.

From a regional point of view, Lombardy has experienced many landslides, due to which, many scholars have regarded landslide susceptibility modeling in different parts of this region (e.g., Valtellina valley (Van Den Eeckhaut et al. 2012)). Yordanov and Brovelli (2020) produced the landslide susceptibility map of the Val Tartano District (Southern Sondrio) using the SI, LR, and RF approaches. Val Tartano is in the right-hand side proximity of the area examined in the present work. They also investigated the effect of partitioning ratio for forming the training and testing databases. A 70/30 ratio was suggested as the most suitable proportion which is the one used in the present study. In a risk assessment effort conducted by Lari et al. (2009) over the Lombardy Region, significant parts of Lecco, particularly coastlines on both sides of the Lake Como and some central parts, fell into high, very high, and extremely high hydrogeological risk (i.e., the risk of landslides along with floods and snow avalanches) (see Figure 6 – (a) of the cited paper). These hazardous parts have many places in common with landslide susceptibile areas recognized in this study.

The findings of this research also compromise with similar studies carried out at national/international levels. It was here discussed that noticing the significant contribution of road networks and gentle terrains in the occurrence of landslides, the study area requires appropriate attention for risk mitigation. In the attention level map suggested by Trigila and Iadanza (2008), the northern part of Lombardy (including the present studied area) demands high and very high attention with respect to the risk of landslide and utilization of land (see Figure 18 of the cited paper).

The results of Europe-wide landslide susceptibility assessment fulfilled by Van Den Eeckhaut, Hervás et al. (2012) showed that the vicinity of Alp Mountains is considerably more susceptible than the rest. Magnification on the obtained map (see Figure 6 – (d) of the cited paper) illustrates that this vicinity includes the north of Italy, and above all, the province of Lecco.

Furthermore, Europe-wide and national-wide landslide susceptibility mappings carried out by Günther et al. (2008) and Trigila et al. (2013), respectively, are in partial accordance with this study. Günther, Reichenbach et al. (2008) presented a probabilistic susceptibility map in which the probability values between 0.8 and 1.00 are most prevalent in the north of Lombardy (see Figure 2 of the cited paper). Similar evaluations can be inferred from the landslide indices calculated by Trigila, Frattini et al. (2013) (see Figure 7 of the cited paper). Also, various global-scale analyses can validate this inference as well (Hong et al. 2007, Stanley and Kirschbaum 2017).

Once again, compared to the case of this study, the maps regarded for the above validation were drawn for much wider extents, i.e., national, continental, and global scales. They mostly provide information for decision-making in such levels (e.g., allocating budgets). Hereupon, they cannot be expected to reflect the same details as the local maps do. For instance, the exact distribution of susceptible/not susceptible properties and habitats needs local-scale investigations.

5.4 Future efforts

Concerning the results of this study, future projects are recommended to focus on a profound landslide risk analysis through assessing the hazard, exposure, and vulnerability over the study area. Proposing mitigation measures (e.g., early warning systems (Pecoraro et al. 2019)) that may reduce the risk of landslide over the populated areas and valuable assets may be another viable subject.

Moreover, several ideas can be regarded to improve prediction efficiency. The betterment can happen in terms of accuracy and problem complexity. Employing optimization techniques for both training of the intelligent models and optimizing the number of conditioning factors would be worth trying. Comparative studies are also of high interest for recognizing more effective intelligent models.

6 Conclusions

Italy, and more particularly Lecco Province, is a landslide-prone area. In this research, reliable susceptibility maps were produced using state-of-the-art models and high-resolution spatial data. The validation of the results reflected good accuracy for all implemented models. However, the MLPNN emerged as a more generalizable predictive tool. The results illustrated a reasonable susceptibility zonation of landslide. Significant areas were jointly recognized as highly susceptible by all three models. There are valuable assets and populated areas falling into this level of susceptibility. Considering the contribution of conditioning factors, it was discussed that slope degree and distance to road factors are expected to be highly regarded for taking mitigation measures. All in all, the findings of this paper can be interesting for alleviating the risk of landslide through land use planning and decision-making within the studied area.

Declarations

Funding: This research received no funding.

Conflicts of interest: The author declares that there is no conflict of financial/non-financial interest.

Acknowledgment

The author would like to acknowledge Territorial Information of Region Lombardy (https://www.geoportale.regione.lombardia.it/en/home) for providing valuable geographic information used as the material in this study.

References

Ahmed, N., et al. (2021). "Spatio-Temporal Assessment of Groundwater Potential Zone in the Drought-Prone Area of Bangladesh Using GIS-Based Bivariate Models." Natural Resources Research: 1-23. https://doi.org/10.1007/s11053-021-09870-0

Akgün, A. and F. Bulut (2007). "GIS-based landslide susceptibility for Arsin-Yomra (Trabzon, North Turkey) region." Environmental geology **51**(8): 1377-1387. https://doi.org/10.1007/s00254-006-0435-6

Al-Abadi, A. M. (2018). "Mapping flood susceptibility in an arid region of southern Iraq using ensemble machine learning classifiers: a comparative study." Arabian Journal of Geosciences **11**(9): 1-19. https://doi.org/10.1007/s12517-018-3584-5

Alajmi, M. S. and A. M. Almeshal (2020). "Prediction and optimization of surface roughness in a turning process using the ANFIS-QPSO method." Materials **13**(13): 2986. https://doi.org/10.3390/ma13132986

Avand, M. and H. Moradi (2021). "Spatial modeling of flood probability using geo-environmental variables and machine learning models, case study: Tajan watershed, Iran." Advances in Space Research **67**(10): 3169-3186. https://doi.org/10.1016/j.asr.2021.02.011

Avtar, R., et al. (2011). "Landslide susceptibility zonation study using remote sensing and GIS technology in the Ken-Betwa River Link area, India." Bulletin of Engineering Geology and the Environment **70**(4): 595-606. https://doi.org/10.1007/s10064-011-0368-5

Ayalew, L. and H. Yamagishi (2005). "The application of GIS-based logistic regression for landslide susceptibility mapping in the Kakuda-Yahiko Mountains, Central Japan." Geomorphology **65**(1-2): 15-31. https://doi.org/10.1016/j.geomorph.2004.06.010

Bonham-Carter, G. F. (1994). "Geographic information systems for geoscientists-modeling with GIS." Computer methods in the geoscientists **13**: 398.

Bui, D. T., et al. (2019). "Spatial pattern analysis and prediction of forest fire using new machine learning approach of Multivariate Adaptive Regression Splines and Differential Flower Pollination optimization: A case study at Lao Cai province (Viet Nam)." Journal of environmental management **237**: 476-487. https://doi.org/10.1016/j.jenvman.2019.01.108

Bui, D. T., et al. (2020). "Comparing the prediction performance of a Deep Learning Neural Network model with conventional machine learning models in landslide susceptibility assessment." Catena **188**: 104426. https://doi.org/10.1016/j.catena.2019.104426

Calvello, M. and G. Pecoraro (2018). "FraneItalia: a catalog of recent Italian landslides." Geoenvironmental Disasters **5**(1): 1-16. https://doi.org/10.1186/s40677-018-0105-5

Can, A., et al. (2019). "Landslide susceptibility mapping at Ovacık-Karabük (Turkey) using different artificial neural network models: comparison of training algorithms." Bulletin of Engineering Geology and the Environment **78**(1): 89-102. https://doi.org/10.1007/s10064-017-1034-3

Catani, F., et al. (2005). "Landslide hazard and risk mapping at catchment scale in the Arno River basin." Landslides **2**(4): 329-342. https://doi.org/10.1007/s10346-005-0021-0

Chawla, A., et al. (2019). "Landslide susceptibility zonation mapping: A case study from Darjeeling District, eastern Himalayas, India." Journal of the Indian Society of Remote Sensing **47**(3): 497-511. https://doi.org/10.1007/s12524-018-0916-6

650 Chen, W., et al. (2017). "A novel hybrid artificial intelligence approach based on the rotation forest ensemble
651 and naïve Bayes tree classifiers for a landslide susceptibility assessment in Langao County, China." Geomatics,
652 Natural Hazards and Risk **8**(2): 1955-1977. https://doi.org/10.1080/19475705.2017.1401560

653 Chen, Z., et al. (2020). "The influence of DEM spatial resolution on landslide susceptibility mapping in the
654 Baxie River basin, NW China." Natural Hazards **101**(3).

655 Cruden, D. M. (1991). "A simple definition of a landslide." Bulletin of the International Association of
656 Engineering Geology-Bulletin de l'Association Internationale de Géologie de l'Ingénieur **43**(1): 27-29.
657 https://doi.org/10.1007/BF02590167

658 Dou, J., et al. (2020). "Different sampling strategies for predicting landslide susceptibilities are deemed less
659 consequential with deep learning." Science of the total environment **720**: 137320.
660 https://doi.org/10.1016/j.scitotenv.2020.137320

661 El-Magd, S. A. A., et al. (2021). "Spatial modeling and susceptibility zonation of landslides using random forest,
662 naïve bayes and K-nearest neighbor in a complicated terrain." Earth Science Informatics: 1-17.
663 https://doi.org/10.1007/s12145-021-00653-y

664 Fabbri, A. G. and A. Patera (2021). "Spatial Uncertainty of Target Patterns Generated by Different Prediction
665 Models of Landslide Susceptibility." Applied Sciences **11**(8): 3341. https://doi.org/10.3390/app11083341

666 Gayen, A., et al. (2019). "Gully erosion susceptibility assessment and management of hazard-prone areas in
667 India using different machine learning algorithms." Science of the total environment **668**: 124-138.
668 https://doi.org/10.1016/j.scitotenv.2019.02.436

669 Günther, A., et al. (2008). Approaches for delineating areas susceptible to landslides in the framework of the
670 European Soil Thematic Strategy. Proceedings of the first world landslide forum, Tokyo, Citeseer.

671 Hong, H., et al. (2018). "Landslide susceptibility mapping using J48 Decision Tree with AdaBoost, Bagging and
672 Rotation Forest ensembles in the Guangchang area (China)." Catena **163**: 399-413.
673 https://doi.org/10.1016/j.catena.2018.01.005

674 Hong, H., et al. (2020). "Introducing a novel multi-layer perceptron network based on stochastic gradient
675 descent optimized by a meta-heuristic algorithm for landslide susceptibility mapping." Science of the total
676 environment **742**: 140549. https://doi.org/10.1016/j.scitotenv.2020.140549

677 Hong, Y., et al. (2007). "Use of satellite remote sensing data in the mapping of global landslide susceptibility."
678 Natural Hazards **43**(2): 245-256. https://doi.org/10.1007/s11069-006-9104-z

679 Hornik, K. (1991). "Approximation capabilities of multilayer feedforward networks." Neural networks **4**(2):
680 251-257. https://doi.org/10.1016/0893-6080(91)90009-T

681 Hornik, K., et al. (1989). "Multilayer feedforward networks are universal approximators." Neural networks
682 **2**(5): 359-366. https://doi.org/10.1016/0893-6080(89)90020-8

683 Hua, Y., et al. (2021). "Dynamic development of landslide susceptibility based on slope unit and deep neural
684 networks." Landslides **18**(1): 281-302. https://doi.org/10.1007/s10346-020-01444-0

685 Huang, F., et al. (2021). "Uncertainty study of landslide susceptibility prediction considering the different
686 attribute interval numbers of environmental factors and different data-based models." Catena **202**: 105250.
687 https://doi.org/10.1016/j.catena.2021.105250

688 Huang, Y. and L. Zhao (2018). "Review on landslide susceptibility mapping using support vector machines."
689 Catena **165**: 520-529. https://doi.org/10.1016/j.catena.2018.03.003

https://www.geoportale.regione.lombardia.it/en/metadati?p_p_id=detailSheetMetadata_WAR_gptmetadataportlet&p_p_lifecycle=0&p_p_state=normal&p_p_mode=view&_detailSheetMetadata_WAR_gptmetadataportlet_uuid=%7B1D4AAE9F-EB7B-4E3E-AB8A-EE29A2211593%7D. Access Date: 23/07/2021

Jacinth Jennifer, J. and S. Saravanan (2021). "Artificial neural network and sensitivity analysis in the landslide susceptibility mapping of Idukki district, India." Geocarto International: 1-23. https://doi.org/10.1080/10106049.2021.1923831

Jang, J.-S. (1993). "ANFIS: adaptive-network-based fuzzy inference system." IEEE transactions on systems, man, and cybernetics **23**(3): 665-685.

Jiang, C., et al. (2021). "Spatial modeling of gully head erosion on the Loess Plateau using a certainty factor and random forest model." Science of the total environment **783**: 147040. https://doi.org/10.1016/j.scitotenv.2021.147040

Kalantar, B., et al. (2018). "Assessment of the effects of training data selection on the landslide susceptibility mapping: a comparison between support vector machine (SVM), logistic regression (LR) and artificial neural networks (ANN)." Geomatics, Natural Hazards and Risk **9**(1): 49-69. https://doi.org/10.1080/19475705.2017.1407368

Kjekstad, O. and L. Highland (2009). Economic and social impacts of landslides. Landslides–disaster risk reduction, Springer**:** 573-587. https://doi.org/10.1007/978-3-540-69970-5_30

Kumar, R. and R. Anbalagan (2016). "Landslide susceptibility mapping using analytical hierarchy process (AHP) in Tehri reservoir rim region, Uttarakhand." Journal of the Geological Society of India **87**(3): 271-286. https://doi.org/10.1007/s12594-016-0395-8

Lari, S., et al. (2009). "Integration of natural and technological risks in Lombardy, Italy." Natural Hazards and Earth System Sciences **9**(6): 2085-2106. https://doi.org/10.5194/nhess-9-2085-2009

Lee, S., et al. (2003). "Landslide susceptibility analysis using GIS and artificial neural network." Earth Surface Processes and Landforms: The Journal of the British Geomorphological Research Group **28**(12): 1361-1376. https://doi.org/10.1002/esp.593

Li, W., et al. (2021). "Stacking ensemble of deep learning methods for landslide susceptibility mapping in the Three Gorges Reservoir area, China." Stochastic Environmental Research and Risk Assessment: 1-22. https://doi.org/10.1007/s00477-021-02032-x

Li, Y. and P. Mo (2019). "A unified landslide classification system for loess slopes: A critical review." Geomorphology **340**: 67-83. https://doi.org/10.1016/j.geomorph.2019.04.020

Lucchese, L. V., et al. (2021). "Mamdani fuzzy inference systems and artificial neural networks for landslide susceptibility mapping." Natural Hazards **106**(3): 2381-2405. https://doi.org/10.1007/s11069-021-04547-6

Mandal, K., et al. (2021). "Applying deep learning and benchmark machine learning algorithms for landslide susceptibility modelling in Rorachu river basin of Sikkim Himalaya, India." Geoscience Frontiers **12**(5): 101203. https://doi.org/10.1016/j.gsf.2021.101203

Mandal, S. P., et al. (2018). "Comparative evaluation of information value and frequency ratio in landslide susceptibility analysis along national highways of Sikkim Himalaya." Spatial Information Research **26**(2): 127-141. https://doi.org/10.1007/s41324-017-0160-0

Maqsoom, A., et al. (2021). "Landslide susceptibility mapping along the China Pakistan Economic Corridor (CPEC) route using multi-criteria decision-making method." Modeling Earth Systems and Environment: 1-15. https://doi.org/10.1007/s40808-021-01226-0

731 Marquardt, D. W. (1963). "An Algorithm for Least-Squares Estimation of Nonlinear Parameters." Journal of
732 the Society for Industrial and Applied Mathematics **11**(2): 431-441. https://doi.org/10.1137/0111030

733 Mathew, J., et al. (2009). "Landslide susceptibility zonation mapping and its validation in part of Garhwal
734 Lesser Himalaya, India, using binary logistic regression analysis and receiver operating characteristic curve
735 method." Landslides **6**(1): 17-26. https://doi.org/10.1007/s10346-008-0138-z

736 Mehrabi, M., et al. (2020). "Optimizing an adaptive neuro-fuzzy inference system for spatial prediction of
737 landslide susceptibility using four state-of-the-art metaheuristic techniques." Sensors **20**(6): 1723.
738 https://doi.org/10.3390/s20061723

739 https://www.geoportale.regione.lombardia.it/en/metadati?p_p_id=detailSheetMetadata_WAR_gptmetad
740 ataportlet&p_p_lifecycle=0&p_p_state=normal&p_p_mode=view&_detailSheetMetadata_WAR_gptmetad
741 ataportlet_uuid=%7BFC06681A-2403-481F-B6FE-5F952DD48BAF%7D. Access Date: 23/07/2021

742 Mirdda, H. A., et al. (2020). "Analysis of bi-variate statistical and multi-criteria decision-making models in
743 landslide susceptibility mapping in lower Mandakini Valley, India." GeoJournal **85**(3): 681-701.
744 https://doi.org/10.1007/s10708-019-09991-3

745 Moayedi, H., et al. (2021). "Quick integrative optimizers for minimizing the error of neural computing in pan
746 evaporation modeling." Engineering with Computers: 1-17. https://doi.org/10.1007/s00366-020-01277-4

747 Moayedi, H., et al. (2019). "Novel hybrids of adaptive neuro-fuzzy inference system (ANFIS) with several
748 metaheuristic algorithms for spatial susceptibility assessment of seismic-induced landslide." Geomatics,
749 Natural Hazards and Risk **10**(1): 1879-1911. https://doi.org/10.1080/19475705.2019.1650126

750 Moayedi, H., et al. (2019). "Modification of landslide susceptibility mapping using optimized PSO-ANN
751 technique." Engineering with Computers **35**(3): 967-984. https://doi.org/10.1007/s00366-018-0644-0

752 Mohajane, M., et al. (2021). "Application of remote sensing and machine learning algorithms for forest fire
753 mapping in a Mediterranean area." Ecological Indicators **129**: 107869.
754 https://doi.org/10.1016/j.ecolind.2021.107869

755 Mokarram, M. and A. R. Zarei (2018). "Landslide susceptibility mapping using fuzzy-AHP." Geotechnical and
756 Geological Engineering **36**(6): 3931-3943. https://doi.org/10.1007/s10706-018-0583-y

757 Moré, J. J. (1978). The Levenberg-Marquardt algorithm: implementation and theory. Numerical analysis,
758 Springer**:** 105-116.

759 Naghibi, S. A., et al. (2016). "GIS-based groundwater potential mapping using boosted regression tree,
760 classification and regression tree, and random forest machine learning models in Iran." Environmental
761 monitoring and assessment **188**(1): 1-27. https://doi.org/10.1007/s10661-015-5049-6

762 Ngo, P. T. T., et al. (2021). "Evaluation of deep learning algorithms for national scale landslide susceptibility
763 mapping of Iran." Geoscience Frontiers **12**(2): 505-519. https://doi.org/10.1016/j.gsf.2020.06.013

764 Nguyen, H., et al. (2019). "Potential of hybrid evolutionary approaches for assessment of geo-hazard landslide
765 susceptibility mapping." Geomatics, Natural Hazards and Risk **10**(1): 1667-1693.
766 https://doi.org/10.1080/19475705.2019.1607782

767 Nhu, V.-H., et al. (2020). "Shallow landslide susceptibility mapping by random forest base classifier and its
768 ensembles in a semi-arid region of Iran." Forests **11**(4): 421. https://doi.org/10.3390/f11040421

769 Nhu, V.-H., et al. (2020). "Shallow landslide susceptibility mapping: A comparison between logistic model
770 tree, logistic regression, naïve bayes tree, artificial neural network, and support vector machine algorithms."

771 International journal of environmental research and public health **17**(8): 2749.
772 https://doi.org/10.3390/ijerph17082749

773 Nsengiyumva, J. B., et al. (2019). "Comparing probabilistic and statistical methods in landslide susceptibility
774 modeling in Rwanda/Centre-Eastern Africa." Science of the total environment **659**: 1457-1472.
775 https://doi.org/10.1016/j.scitotenv.2018.12.248

776 Oh, H.-J. and B. Pradhan (2011). "Application of a neuro-fuzzy model to landslide-susceptibility mapping for
777 shallow landslides in a tropical hilly area." Computers & Geosciences **37**(9): 1264-1276.
778 https://doi.org/10.1016/j.cageo.2010.10.012

779 Ozdemir, A. (2011). "GIS-based groundwater spring potential mapping in the Sultan Mountains (Konya,
780 Turkey) using frequency ratio, weights of evidence and logistic regression methods and their comparison."
781 Journal of Hydrology **411**(3-4): 290-308. https://doi.org/10.1016/j.jhydrol.2011.10.010

782 Ozdemir, A. and T. Altural (2013). "A comparative study of frequency ratio, weights of evidence and logistic
783 regression methods for landslide susceptibility mapping: Sultan Mountains, SW Turkey." Journal of Asian
784 Earth Sciences **64**: 180-197. https://doi.org/10.1016/j.jseaes.2012.12.014

785 Panahi, M., et al. (2020). "Spatial prediction of landslide susceptibility using hybrid support vector regression
786 (SVR) and the adaptive neuro-fuzzy inference system (ANFIS) with various metaheuristic algorithms." Science
787 of the total environment **741**: 139937. https://doi.org/10.1016/j.scitotenv.2020.139937

788 Pandey, V. K., et al. (2021). "Implications of landslide inventory in susceptibility modeling along a Himalayan
789 highway corridor, India." Physical Geography: 1-24. https://doi.org/10.1080/02723646.2021.1872857

790 Parente, F., et al. (2013). "Outcomes and cost evaluation of the first two rounds of a colorectal cancer
791 screening program based on immunochemical fecal occult blood test in northern Italy." Endoscopy **45**(01):
792 27-34. https://doi.org/10.1055/s-0032-1325800

793 Park, S., et al. (2013). "Landslide susceptibility mapping using frequency ratio, analytic hierarchy process,
794 logistic regression, and artificial neural network methods at the Inje area, Korea." Environmental earth
795 sciences **68**(5): 1443-1464. https://doi.org/10.1007/s12665-012-1842-5

796 Pecoraro, G., et al. (2019). "Monitoring strategies for local landslide early warning systems." Landslides **16**(2):
797 213-231. https://doi.org/10.1007/s10346-018-1068-z

798 Pham, B. T., et al. (2018). "Spatial prediction of landslides using a hybrid machine learning approach based
799 on random subspace and classification and regression trees." Geomorphology **303**: 256-270.
800 https://doi.org/10.1016/j.geomorph.2017.12.008

801 Pham, B. T., et al. (2019). "A comparison of Support Vector Machines and Bayesian algorithms for landslide
802 susceptibility modelling." Geocarto International **34**(13): 1385-1407.
803 https://doi.org/10.1080/10106049.2018.1489422

804 Pham, Q. B., et al. (2021). "A comparison among fuzzy multi-criteria decision making, bivariate, multivariate
805 and machine learning models in landslide susceptibility mapping." Geomatics, Natural Hazards and Risk **12**(1):
806 1741-1777. https://doi.org/10.1080/19475705.2021.1944330

807 Pokharel, B., et al. (2021). "Spatial clustering and modelling for landslide susceptibility mapping in the north
808 of the Kathmandu Valley, Nepal." Landslides **18**(4): 1403-1419. https://doi.org/10.1007/s10346-020-01558-
809 5

810 Pourghasemi, H. R., et al. (2013). "Landslide susceptibility mapping using support vector machine and GIS at
811 the Golestan Province, Iran." Journal of Earth System Science **122**(2): 349-369.
812 https://doi.org/10.1007/s12040-013-0282-2

Pourghasemi, H. R., et al. (2012). "Landslide susceptibility mapping using index of entropy and conditional probability models in GIS: Safarood Basin, Iran." Catena **97**: 71-84. https://doi.org/10.1016/j.catena.2012.05.005

Pourtaghi, Z. S., et al. (2015). "Forest fire susceptibility mapping in the Minudasht forests, Golestan province, Iran." Environmental earth sciences **73**(4): 1515-1533. https://doi.org/10.1007/s12665-014-3502-4

Pradhan, B. and S. Lee (2010). "Regional landslide susceptibility analysis using back-propagation neural network model at Cameron Highland, Malaysia." Landslides **7**(1): 13-30. https://doi.org/10.1007/s10346-009-0183-2

Pradhan, B., et al. (2010). "A GIS-based back-propagation neural network model and its cross-application and validation for landslide susceptibility analyses." Computers, Environment and Urban Systems **34**(3): 216-235. https://doi.org/10.1016/j.compenvurbsys.2009.12.004

Pradhan, S. P. and T. Siddique (2020). "Stability assessment of landslide-prone road cut rock slopes in Himalayan terrain: a finite element method based approach." Journal of Rock Mechanics and Geotechnical Engineering **12**(1): 59-73. https://doi.org/10.1016/j.jrmge.2018.12.018

Razavi-Termeh, S. V., et al. (2021). "Mapping of landslide susceptibility using the combination of neuro-fuzzy inference system (ANFIS), ant colony (ANFIS-ACOR), and differential evolution (ANFIS-DE) models." Bulletin of Engineering Geology and the Environment **80**(3): 2045-2067. https://doi.org/10.1007/s10064-020-02048-7

Regmi, A. D., et al. (2014). "Application of frequency ratio, statistical index, and weights-of-evidence models and their comparison in landslide susceptibility mapping in Central Nepal Himalaya." Arabian Journal of Geosciences **7**(2): 725-742. https://doi.org/10.1007/s12517-012-0807-z

Reichenbach, P., et al. (2018). "A review of statistically-based landslide susceptibility models." Earth-Science Reviews **180**: 60-91. https://doi.org/10.1016/j.earscirev.2018.03.001

Sadighi, M., et al. (2020). "Assessing landslide susceptibility using machine learning models: a comparison between ANN, ANFIS, and ANFIS-ICA." Environmental earth sciences **79**(24): 1-14. https://doi.org/10.1007/s12665-020-09294-8

Saha, A. and S. Saha (2021). "Application of statistical probabilistic methods in landslide susceptibility assessment in Kurseong and its surrounding area of Darjeeling Himalayan, India: RS-GIS approach." Environment, Development and Sustainability **23**: 4453-4483. https://doi.org/10.1007/s10668-020-00783-1

Saha, S., et al. (2021). "Prediction of landslide susceptibility in Rudraprayag, India using novel ensemble of conditional probability and boosted regression tree-based on cross-validation method." Science of the total environment **764**: 142928. https://doi.org/10.1016/j.scitotenv.2020.142928

Sahin, E. K. (2020). "Comparative analysis of gradient boosting algorithms for landslide susceptibility mapping." Geocarto International: 1-25. https://doi.org/10.1080/10106049.2020.1831623

Seyedashraf, O., et al. (2018). "Novel approach for dam break flow modeling using computational intelligence." Journal of Hydrology **559**: 1028-1038. https://doi.org/10.1016/j.jhydrol.2018.03.001

Singh, K. and V. Kumar (2018). "Hazard assessment of landslide disaster using information value method and analytical hierarchy process in highly tectonic Chamba region in bosom of Himalaya." Journal of Mountain science **15**(4).

Stanley, T. and D. B. Kirschbaum (2017). "A heuristic approach to global landslide susceptibility mapping." Natural Hazards **87**(1): 145-164. https://doi.org/10.1007/s11069-017-2757-y

Sterlacchini, S., et al. (2011). "Spatial agreement of predicted patterns in landslide susceptibility maps." Geomorphology **125**(1): 51-61. https://doi.org/10.1016/j.geomorph.2010.09.004

Sun, D., et al. (2020). "A random forest model of landslide susceptibility mapping based on hyperparameter optimization using Bayes algorithm." Geomorphology **362**: 107201. https://doi.org/10.1016/j.geomorph.2020.107201

Tangestani, M. H. (2009). "A comparative study of Dempster–Shafer and fuzzy models for landslide susceptibility mapping using a GIS: An experience from Zagros Mountains, SW Iran." Journal of Asian Earth Sciences **35**(1): 66-73. https://doi.org/10.1016/j.jseaes.2009.01.002

Tehrany, M. S., et al. (2019). "A novel ensemble modeling approach for the spatial prediction of tropical forest fire susceptibility using LogitBoost machine learning classifier and multi-source geospatial data." Theoretical and Applied Climatology **137**(1): 637-653. https://doi.org/10.1007/s00704-018-2628-9

Termeh, S. V. R., et al. (2018). "Flood susceptibility mapping using novel ensembles of adaptive neuro fuzzy inference system and metaheuristic algorithms." Science of the total environment **615**: 438-451. https://doi.org/10.1016/j.scitotenv.2017.09.262

Thai Pham, B., et al. (2019). "Landslide susceptibility assessment by novel hybrid machine learning algorithms." Sustainability **11**(16): 4386. https://doi.org/10.3390/su11164386

Trigila, A., et al. (2013). Landslide susceptibility mapping at national scale: the Italian case study. Landslide science and practice, Springer**:** 287-295. https://doi.org/10.1007/978-3-642-31325-7_38

Trigila, A. and C. Iadanza (2008). Landslides in Italy, Italian National Institute for Environmental Protection and Research (ISPRA).

Trigila, A., et al. (2010). "Quality assessment of the Italian Landslide Inventory using GIS processing." Landslides **7**(4): 455-470. https://doi.org/10.1007/s10346-010-0213-0

Vahidnia, M. H., et al. (2010). "A GIS-based neuro-fuzzy procedure for integrating knowledge and data in landslide susceptibility mapping." Computers & Geosciences **36**(9): 1101-1114. https://doi.org/10.1016/j.cageo.2010.04.004

Van Den Eeckhaut, M., et al. (2012). "Statistical modelling of Europe-wide landslide susceptibility using limited landslide inventory data." Landslides **9**(3): 357-369. https://doi.org/10.1007/s10346-011-0299-z

Varnes, D. J. (1984). Landslide hazard zonation: a review of principles and practice.

Wei, A., et al. (2021). "A novel combination approach for karst collapse susceptibility assessment using the analytic hierarchy process, catastrophe, and entropy model." Natural Hazards **105**(1): 405-430. https://doi.org/10.1007/s11069-020-04317-w

Wu, X., et al. (2013). "Landslide susceptibility mapping using rough sets and back-propagation neural networks in the Three Gorges, China." Environmental earth sciences **70**(3): 1307-1318. https://doi.org/10.1007/s12665-013-2217-2

https://en.climate-data.org/europe/italy/lombardy/lecco-1099/. Access Date: 23/07/2021

https://www.geoportale.regione.lombardia.it/en/metadati?p_p_id=detailSheetMetadata_WAR_gptmetadataportlet&p_p_lifecycle=0&p_p_state=normal&p_p_mode=view&_detailSheetMetadata_WAR_gptmetadataportlet_uuid=%7B7BDF78CD-C179-472F-96BE-072A0EBB6C76%7D. Access Date: 23/07/2021

https://www.geoportale.regione.lombardia.it/en/home. Access Date: 23/07/2021

https://land.copernicus.eu/pan-european/corine-land-cover. Access Date: 23/07/2021

https://www.worldweatheronline.com/lecco-weather-averages/lombardia/it.aspx. Access Date: 23/07/2021

Xiao, T., et al. (2019). "Spatial prediction of landslide susceptibility using GIS-based statistical and machine learning models in Wanzhou County, Three Gorges Reservoir, China." Acta Geochimica **38**(5): 654-669.

Yalcin, A. (2008). "GIS-based landslide susceptibility mapping using analytical hierarchy process and bivariate statistics in Ardesen (Turkey): comparisons of results and confirmations." Catena **72**(1): 1-12. https://doi.org/10.1016/j.catena.2007.01.003

Yalcin, A., et al. (2011). "A GIS-based comparative study of frequency ratio, analytical hierarchy process, bivariate statistics and logistics regression methods for landslide susceptibility mapping in Trabzon, NE Turkey." Catena **85**(3): 274-287. https://doi.org/10.1016/j.catena.2011.01.014

Yi, Y., et al. (2020). "Landslide susceptibility mapping using multiscale sampling strategy and convolutional neural network: A case study in Jiuzhaigou region." Catena **195**: 104851. https://doi.org/10.1016/j.catena.2020.104851

Yilmaz, I. (2009). "Landslide susceptibility mapping using frequency ratio, logistic regression, artificial neural networks and their comparison: a case study from Kat landslides (Tokat—Turkey)." Computers & Geosciences **35**(6): 1125-1138. https://doi.org/10.1016/j.cageo.2008.08.007

Yilmaz, I. (2010). "The effect of the sampling strategies on the landslide susceptibility mapping by conditional probability and artificial neural networks." Environmental earth sciences **60**(3): 505-519. https://doi.org/10.1007/s12665-009-0191-5

Yordanov, V. and M. A. Brovelli (2020). "Application of various strategies and methodologies for landslide susceptibility maps on a basin scale: the case study of Val Tartano, Italy." Applied Geomatics: 1-23. https://doi.org/10.1007/s12518-020-00344-1

Yoshimatsu, H. and S. Abe (2006). "A review of landslide hazards in Japan and assessment of their susceptibility using an analytical hierarchic process (AHP) method." Landslides **3**(2): 149-158. https://doi.org/10.1007/s10346-005-0031-y

Youssef, A. M. and H. R. Pourghasemi (2021). "Landslide susceptibility mapping using machine learning algorithms and comparison of their performance at Abha Basin, Asir Region, Saudi Arabia." Geoscience Frontiers **12**(2): 639-655. https://doi.org/10.1016/j.gsf.2020.05.010

Zabihi, M., et al. (2018). "Spatial modelling of gully erosion in Mazandaran Province, northern Iran." Catena **161**: 1-13. https://doi.org/10.1016/j.catena.2017.10.010

Zheng, S., et al. (2020). "Early prediction of cooling load in energy-efficient buildings through novel optimizer of shuffled complex evolution." Engineering with Computers: 1-15. https://doi.org/10.1007/s00366-020-01140-6